1974-12

Ray trace experiment on the underwater range at Dabob Bay

Karon, Stuart Charles

Monterey, California. Naval Postgraduate School

RAY TRACE EXPERIMENT ON THE UNDERWATER RANGE AT DABOB BAY

Stuart Charles Karon

NAVAL POSTGRADUATE SCHOOL
Monterey, California

THESIS

RAY TRACE EXPERIMENT ON THE
UNDERWATER RANGE AT DABOB BAY

by

Stuart Charles Karon

December 1974

Thesis Advisor: J.V. Sanders

Approved for public release; distribution unlimited.

REPORT DOCUMENTATION PAGE

READ INSTRUCTIONS BEFORE COMPLETING FORM

1. REPORT NUMBER

2. GOVT ACCESSION NO.

3. RECIPIENT'S CATALOG NUMBER

4. TITLE (and Subtitle)
Ray Trace Experiment on the Underwater Range at Dabob Bay

5. TYPE OF REPORT & PERIOD COVERED
Master's Thesis; December 1974

6. PERFORMING ORG. REPORT NUMBER

7. AUTHOR(s)
Stuart Charles Karon

8. CONTRACT OR GRANT NUMBER(s)

9. PERFORMING ORGANIZATION NAME AND ADDRESS
Naval Postgraduate School
Monterey, California 93940

10. PROGRAM ELEMENT, PROJECT, TASK AREA & WORK UNIT NUMBERS

11. CONTROLLING OFFICE NAME AND ADDRESS
Naval Postgraduate School
Monterey, California 93940

12. REPORT DATE
December 1974

13. NUMBER OF PAGES
84

14. MONITORING AGENCY NAME & ADDRESS(if different from Controlling Office)
Naval Postgraduate School
Monterey, California 93940

15. SECURITY CLASS. (of this report)
Unclassified

15a. DECLASSIFICATION/DOWNGRADING SCHEDULE

16. DISTRIBUTION STATEMENT (of this Report)
Approved for public release; distribution unlimited.

17. DISTRIBUTION STATEMENT (of the abstract entered in Block 20, if different from Report)

18. SUPPLEMENTARY NOTES

19. KEY WORDS (Continue on reverse side if necessary and identify by block number)
Ray-Tracing
Underwater Range
Dabob Bay
Keyport, Washington

20. ABSTRACT (Continue on reverse side if necessary and identify by block number)
Preliminary results of an experiment to determine the accuracy and the effects of varying amounts of environmental data at the NAVTORPSTA, Keyport, Washington, Dabob Bay Range are presented. A 75-KHz source was tracked at six depths at each of six horizontal ranges. The data were analyzed by the NAVTORPSTA NUTRACK III isovelocity-layer computer program and by an isogradient-layer program developed here, STUTRACK I. The results show that a low signal-to-noise ratio is not a

(20. ABSTRACT Continued)

problem even at long distances and that an isogradient analysis yields superior results with less environmental data than does the isovelocity method.

Ray Trace Experiment on the Underwater Range at Dabob Bay

by

Stuart Charles Karon
Lieutenant, United States Navy
B.A., University of Minnesota, 1968

Submitted in partial fulfillment of the
requirements for the degree of

MASTER OF SCIENCE IN ENGINEERING ACOUSTICS

from the

NAVAL POSTGRADUATE SCHOOL
December 1974

ABSTRACT

Preliminary results of an experiment to determine the accuracy and the effects of varying amounts of environmental data at the NAVTORPSTA, Keyport, Washington, Dabob Bay Range are presented. A 75-KHz source was tracked at six depths at each of six horizontal ranges. The data were analyzed by the NAVTORPSTA NUTRACK III isovelocity-layer computer program and by an isogradient-layer program developed here, STUTRACK I. The results show that a low signal-to-noise ratio is not a problem even at long distances and that an isogradient analysis yields superior results with less environmental data than does the isovelocity method.

TABLE OF CONTENTS

LIST OF ILLUSTRATIONS

ACKNOWLEDGEMENTS

The author wishes to express his appreciation to Professor James V. Sanders of the Department of Physics, U. S. Naval Postgraduate School, for his firm guidance, suggestions, and patience throughout the course of this project; and to Professors Alan B. Coppens and Harvey A. Dahl for valuable conversations.

In addition the writer is indebted to the personnel of the Naval Torpedo Station, Keyport, Washington, for without their cooperation this project would not have been possible.

I. INTRODUCTION

A. DABOB BAY FACILITY

A facility for the three-dimensional tracking of surface ships, submarines, and torpedoes is located at the Dabob Bay facility of the Naval Torpedo Station (NAVTORPSTA), Keyport, Washington. Chosen because of its favorable oceanographic features and its proximity to the NAVTORPSTA, Keyport, Dabob Bay has been used for torpedo testing since 1949. It consists of a 250-KHz "high frequency" installation no longer operating, and a 75-KHz "low frequency" primary tracking system enveloping nearly the entire bay providing for underwater tracking in a volume approximately 30,000 feet by 4,500 feet by 600 feet deep.

Dabob Bay, a branch of Hood Canal, is in a deep (600 feet) depression adjacent to the Olympic Mountains. The Quilcene River flows into the northernmost part and the Dosewallips River into the southernmost. The sides of the bay are precipitous and predominately rocky, while the bottom is mud. Annual precipitation averages about 51 inches and while average snowfall is about 15 inches, any one snowfall seldom remains longer than a few days. Winds generally blow along the length of Dabob Bay; i.e., North and South. Southerly winds are usually accompanied by clear skies and occur most often in summer. Normal wind velocities are

5 to 15 miles per hour. Tidal levels in Dabob Bay range from about -5 to +15 feet.

Water temperatures change markedly from season to season and even from day to day. The changes are most noticeable near the surface but may be observed even at greater depths. Salinity varies considerably with depth as fresher surface water from terrestrial runoff overlays more saline water. The variation is also quite seasonal, reaching a maximum in the spring. The main contributor to sound velocity changes is water temperature, and the resulting sound velocity profile is representative of the temperature gradient.

B. MOTIVATION

NAVTORPSTA, Keyport, has developed a computer program, NUTRACK III, which divides the bay into laterally homogeneous, isovelocity layers and traces a sound ray from a three-dimensional hydrophone array mounted just above the bottom, back to its source.

An experiment was undertaken to provide comparison of the three-dimensional position of a source with respect to a receiver as determined by various ray-tracing techniques. From this comparison it was hoped that an optimum ray-trace procedure would be indicated and that a better understanding of the significance of environmental variations would result.

II. PROCEDURE

A. DETAILED RANGE DESCRIPTION

The basic underwater tracking system on the 75-KHz range is comprised of three components: hydrophone array, computer system, and vehicular instrumentation. The ship-board transducer emits a 75-KHz acoustic pulse in synchronism with a master clock at the computer site. This pulse is detected by each of the four hydrophones (R_x,R_y,R_z and R_c) in the array and mixed with a local oscillator having a frequency unique to that hydrophone. The outputs of these oscillators are preamplified and fed to a multiplexer, which sums the signals and transmits the composite signal via an underwater cable to the computer site, where it is processed to determine the in-water transit time to each hydrophone (T_x,T_y,T_z, and T_c).

1. Hydrophone Array Configuration

The hydrophones in the NAVTORPSTA Range are arranged in a short-baseline system in groups of four, each one located on each of four adjacent corners in an imaginary 30-foot cube, thereby defining the orthogonal coordinate system in which the measurements were made. These hydrophone arrays used buoyant spheres which exert an upward force in excess of two thousand pounds to keep them upright. The array is not free to rotate about the Z axis, but may tilt as much as two degrees from the horizontal in strong currents.

This tilt is measured by servo-pendulum transducers whose specified resolution is 0.00833 degrees, accuracy 0.025 degrees, and linearity 0.05 percent over the full scale.

The Range consists of six arrays (Fig. 1) aligned along a line 450 feet east and parallel to the Range axis, spaced at 6000-foot intervals, with the 00 array being the farthest north. The Range axis is 191° 18' 14.1" T.

2. Computer System

The computer system, a Scientific Data Systems (SDS) model 920, is installed on Zelatched Point and consists of three main subsystems: the signal processing subsystem, the data collection subsystem, and the computer subsystem. The signal processing subsystem, the link between the hydrophones and the data collection subsystem, processes the multiplexed signal received from the arrays, discriminates against unwanted signals, and determines the in-water transit time to each hydrophone. The data collection subsystem establishes the master clock timing by which all timing is computed. It also prepares all the array signals for the computer subsystem, which calculates the tracked object's position, prints the tracking data, and records the data on magnetic tape. For real-time examination, the data are plotted on X-Y plotters.

B. EXPERIMENTAL PROCEDURE

A 92.5 dB acoustic source with approximately ten pounds of ballast was suspended from the stern of the sound boat to 25, 50, 75, 100, 150, and 200-foot depths at six

horizontal ranges (stations) from 900 feet to 4700 feet from the 02 hydrophone (Fig. 2). The first station was located approximately 900 feet north of hydrophone array 02, and 450 feet east of the Range axis. Successive stations were located parallel to the axis of the Range; the second being directly over the array, the third 600 feet past it (diametrically opposite the first station), and then at about 1500-foot intervals to about 4500 feet, beyond which signal-to-noise problems made further examination impossible. The source emitted one 1.3 millesecond 75-KHz pulse per second for sixty to ninety seconds at each depth at each station.

The position of the boat on the Range was found in the horizontal from the Range's Autotape system, a portable and commercial microwave system used exclusively for ship tracking that yields accuracies of ±3 feet. The position of the acoustic source with respect to the Autotape antenna was determined from the length of cable let out, the horizontal distance from the antenna to the stern of the boat, and the boat's heading. Tidal data were recorded and used for correcting depth coordinates to a mean low-low water (0-foot tide) reference plane. The array is known to be 585 feet below MLLW, so that the depth of the source below the surface and the tide measurement allows calculation of the vertical distance between the source and array. All measurements were made with respect to the array's coordinate system, although the array's orientation and location on the

Range were known, making it possible to transform this data to a true position on the Range. The X axis of the 02 array was 25° 24' 36.0" T.

A NAVTORPSTA digital velocimeter that has an accuracy to ±1.0 ft/sec and resolution of ±0.7 ft/sec measured the sound-velocity profile at each station. NAVTORPSTA instrumentation at Dabob Bay measured and recorded the acoustic travel times from the source to each of the four hydrophones in the array to six decimal places for every source depth at each station. The three-dimensional position of the source with respect to the array was calculated from these travel times by the NAVTORPSTA NUTRACK III computer program.

The data were gathered on 21 March, 1974 during a neap tidal period and while the sea surface was smooth and glassy, although there had been ripples earlier in the morning. The day was bright and sunny with scattered, thin, high overcast, the temperature was 55°F, and no noticeable wind was present. The shiny stainless steel transducer disappeared from view when about eight feet deep, indicative of thick biological concentrations (gelbstaffen) in the water. Rudimentary drift measurements of boat movement relative to surface water were taken by throwing paper into the water and watching its relative motion with respect to the boat, which indicated a value of approximately 0.3 ft/sec.

III. THEORETICAL DEVELOPMENT

The computer program analysis includes corrections for the fact that acoustic rays are not straight lines in a non-homogeneous medium. Two simple ray-tracing techniques exist: the water mass divided into layers of isovelocity water or into layers with a constant velocity gradient. The isovelocity method is employed in the NAVTORPSTA NUTRACK III program; while employment of the isogradient technique is one of the purposes of this present experiment.

A. NUTRACK III

1. Raw Array Coordinates

The geometry involved in the calculations of the raw array coordinates is shown in Fig. 3. As described earlier, the four hydrophones are on four adjacent vertices separated by a distance d, along the edge of the cube. The origin, 0, of the array coordinates is at the center of the cube with the orthogonal coordinates parallel to its edge. Let the transit times of the acoustic pulse from the tracked source to the c hydrophone and the Y hydrophone be T_c and T_y, respectively, then

$$(cT_c)^2 = (RAWY + \frac{d}{2})^2 + (RAWX + \frac{d}{2})^2 + (RAWZ + \frac{d}{2})^2 \qquad (1)$$

and

$$(cT_y)^2 = (RAWY - \frac{d}{2})^2 + (RAWX + \frac{d}{2})^2 + (RAWZ + \frac{d}{2})^2 \ . \qquad (2)$$

Taking the difference between T_c^2 and T_y^2, expanding, and combining terms yields

$$RAWY = \frac{c^2}{2d} (T_c + T_y)(T_c - T_y) \quad . \tag{3}$$

In similar fashion, analogous expressions may be obtained for the X and Z coordinates:

$$RAWX = \frac{c^2}{2d} (T_c + T_x)(T_c - T_x) \tag{4}$$

and

$$RAWZ = \frac{c^2}{2d} (T_c + T_z)(T_c - T_z) \quad , \tag{5}$$

where

c = the average sound velcoity, about 4860 ft/sec;
d = the distance between hydrophones, 30 ft;
T_c, T_x, T_y, T_z = travel times in seconds.

The travel times are determined from a clock whose period is 0.4×10^{-6} sec. (2.5 mHz), which is sufficiently high to measure precisely the arrival time of a 75-kHz signal (about 8 counts per quarter period). A correction factor must be applied to correct for the array receiver integration (pulse width descrimination). Let

I = the integration time, 800 μs
T'_c = the measured travel time to the R_c hydrophone;
T_c = actual travel time,

so that

$$T'_c = T_c + I \quad ,$$

$$T'_y = T_y + I \quad ,$$

and

$$T_c + T_y = (T'_c + T'_y - 2I) \quad ,$$

$$T_c - T_y = T'_c - T'_y \quad .$$

The relations for the raw coordinates are now

$$RAWY = \frac{c^2}{2d} (T'_c + T'_y - K)(T'_c - T'_y) \quad , \tag{6}$$

where $K = 2I = 1.6 \times 10^{-3}$ sec and T'_c and T'_y are the measured times.

Similarly

$$RAWX = \frac{c^2}{2d} (T'_c + T'_y - K)(T'_c - T'_x) \tag{7}$$

and

$$RAWZ = \frac{c^2}{2d} (T'_c + T'_z - K)(T'_c - T'_z) \quad . \tag{8}$$

2. Tilt Correction to Determine Corrected Array Coordinates

The raw coordinates previously computed are referenced to a non-horizontal reference plane. The array is instrumented to sense the angles the array axes make with the horizontal, called XTILT, or rotation about the Y axis, and YTILT, or rotation about the X axis, respectively.

These are given from

$$XTILT = (TILTX - 505) \times .00833 \text{ degrees}$$

and

$$YTILT = (TILTY - 505) \times .00833 \text{ degrees}$$

where TILTX and TILTY are sensor outputs and 505 is an arbitrarily determined sensor reading for a perfectly horizontal orientation.

The correction of RAW coordinates for array tilt is merely a matter of geometry. Figure 4 shows that

$$CORX = [RAWX][COS(XTILT)] = [RAWZ][SIN(XTILT)]. \quad (9)$$

Since XTILT is small, it may be assumed that COS(XTILT) = 1. The relationship then becomes

$$CORX = RAWX - [RAWZ][SIN(XTILT)] \quad . \quad (10)$$

Similarly

$$CORY = RAWY - [RAWZ][SIN(YTILT)] \quad (11)$$

and

$$CORZ = RAWZ + [RAWX][SIN(XTILT)] + [RAWY][SIN(YTILT)] \quad . \quad (12)$$

These relationships are valid for both positive and negative tilt as the SIN term also changes sign to maintain the relationship.

3. Ray Path Refraction

In a homogeneous body of water, the minimum time path between an output transducer and receiving hydrophone is a straight line. When the speed of propagation is spatially varying due to temperature and salinity variations, refraction occurs and the minimum time path is no longer a straight line. Corrections must then be made to determine the true position of the source.

From the classical laws of Fermat and Snell, a minimum-time path is computed, working back in time from the array center in the direction of the "apparent" position and tracing the array through each velocity layer. The process is continued upward in space and backward in time until the measured travel time is consumed. To determine ray-path refraction, the sound speed is taken at one-foot increments and averaged over ten feet. Since the array depth is 585 feet, there are 58 ten-foot layers and one five-foot layer. The vertical angle of entry of the ray at the array, computed from the tilt-corrected array coordinates (Fig. 5), is

$$A_o = \mathrm{SIN}^{-1} \left[\frac{\mathrm{CORZ}^2}{\mathrm{CORX}^2 + \mathrm{CORY}^2 + \mathrm{CORZ}^2} \right]^{1/2} . \qquad (13)$$

The entry angle A_o computed from the CORR array coordinates is assumed to be equal to the entry angle for the minimum time path. This assumption is good if the source is far enough so that the wave fronts are plane over

the dimensions of the array, and the speed of sound is constant over the dimensions of the array.

The travel time, T, to the origin is computed from

$$\frac{T}{T_c} = \frac{S}{R_c} \quad , \tag{14}$$

where

$$S = [CORX^2 + CORY^2 + CORZ^2]^{1/2} \tag{15}$$

and

$$R_c = [(CORX + 15)^2 + (CORY + 15)^2 + (CORZ + 15)^2]^{1/2} \quad , \tag{16}$$

where R_c is the slant range to the C array hydrophone, and S is the slant range to the array center.

It may be seen that the assumption of an average velocity, c, in computing RAWX, RAWY, RAWZ is not sensitive as the ratio of S to R_c is what is really important and any small error will tend to cancel out.

The horizontal distance is

$$H = [CORX^2 + CORY^2]^{1/2} \quad . \tag{17}$$

The first layer processed is between the deepest depth in the velocity profile that is shallower than the array, and the array itself;

$$\Delta Z_1 = A_d - Z_1 \quad , \tag{18}$$

where A_d is the array depth.

The incremental slant range is

$$\Delta S_1 = \frac{\Delta Z_1}{\text{SIN } A_o} \quad . \tag{19}$$

The incremental travel time in this layer, used to increment the pulse travel time T, is

$$\Delta T = \frac{\Delta S_1}{c_1} \quad , \tag{20}$$

where c_1 is the average velocity in the layer. This incremental travel time is used to decrement the pulse travel time T. The horizontal distance for this time is

$$\Delta H_1 = \Delta S_1 \text{ COS } A_o \quad . \tag{21}$$

The values ΔH and ΔZ are accumulated as the time clock is decremented layer by layer.

Using Snell's law, the change in angle due to refraction upon entry into a new velocity layer is

$$\frac{\text{COS } A_o}{\text{COS}(A_o + \Delta A)} = \frac{c_1}{c_2}$$

or

$$\text{COS } A_1 = \text{COS } A_o \frac{c_2}{c_1} \tag{22}$$

where

$$A_1 = A_o + \Delta A$$

and

$$\text{SIN } A_1 = (1 - \text{COS}^2 A_1)^{1/2} \qquad (23)$$

The thickness of the layer is

$$\Delta Z_2 = Z_2 - Z_1 \quad . \qquad (24)$$

This process is repeated and the original travel time T is decremented with the incremental layer travel times until T is consumed. The ray-bent X, Y, and Z (RBNX, RBNY, RBNZ) are

$$\text{RBNX} = \left(\frac{\text{CORX}}{H} \right) \Sigma \Delta H \quad , \qquad (25)$$

$$\text{RBNY} = \left(\frac{\text{CORY}}{H} \right) \Sigma \Delta H \quad , \qquad (26)$$

and

$$\text{RBNZ} = \Sigma \Delta Z \qquad (27)$$

This raypath migration process assumes a laterally homogeneous medium within the neighborhood of each array. Independent velocity profiles are not taken at each array.

This will introduce small discontinuities in track as the tracked vehicle is passed from one array to another.

4. Error Estimation

Returning to Eq. 4, and assuming equal errors, $\Delta T_c = \Delta T_x = \Delta t$ in time measurement; the maximum expected error in RBNX (ΔX) is found from

$$RAWX + \Delta X = \frac{c^2}{2d} [(T_c + \Delta t)^2 - (T_x - \Delta t)^2]$$

$$= \frac{c^2}{2d} [T_c^2 - T_x^2] + \frac{c^2}{d} [T_c \Delta t + T_x \Delta t] \qquad (28)$$

to be

$$\Delta X \doteq \frac{c^2}{d} [T_c + T_x] \Delta t \quad . \qquad (29)$$

At large ranges, $T_c \approx T_x$, so

$$\Delta X = \frac{2c^2}{d} T_c \Delta t \quad ,$$

but $c \cdot T_c = R$, so

$$\frac{\Delta X}{R} \doteq 2 \left(\frac{c}{d}\right) \Delta t \quad . \qquad (30)$$

Similarly,

$$\frac{\Delta Y}{R} \doteq 2 \left(\frac{c}{d}\right) \Delta t \qquad (31)$$

and

$$\frac{\Delta Z}{R} \doteq 2 \left(\frac{c}{d}\right) \Delta t \quad . \qquad (32)$$

Assuming the maximum error in time is one-fourth of the period of the 75-kHz signal, $\Delta T_c \approx 3.3 \times 10^{-6}$ sec, so

$$\frac{\Delta X}{R} \approx \frac{\Delta Y}{R} \approx \frac{\Delta Z}{R} \approx 1 \times 10^{-3} \quad .$$

B. ISOGRADIENT PROGRAM "STUTRACK I"

An isogradient computer program, STUTRACK I, was developed for comparison with NUTRACK III.

1. Linear Gradient Theory

Figure 6 shows a highly exaggerated speed of sound profile which has been approximated by two layers each possessing a constant gradient. In each layer, the speed of sound may be given as

$$c(Z) = c_o + G\Delta Z \qquad (33)$$

where G is the gradient; G is negative in the upper layer and positive in the lower layer. Applying Snell's Law for A,

$$\frac{\cos A}{c} = \text{CONSTANT} \quad , \qquad (34)$$

one may see that the raypath curves downward in the upper layer and upward in the lower layer. Let the radius of curvature for the arc between the angles A_1 and A_2 in the upper layer be R. Then

$$\Delta Z = R(\cos A_1 - \cos A_2) = R \cos A_1 \left(\frac{c_1 - c_2}{c_1}\right) . \qquad (35)$$

However, from Eq. 33,

$$c_1 - c_2 = -G\Delta Z$$

and with Eq. 34,

$$R = \frac{-1}{G} \frac{c}{\cos A} . \qquad (36)$$

Thus for each raypath the value of R is a constant in a linear gradient layer, and the path is an arc of a circle. The center of the circle lies at the depth for which A would become 90° if the sound profile for the upper layer were to descend to greater depths.

Assuming that the initial angle of depression of the raypath is A_o, from the geometry of Fig. 6 and with Eq. 36, the change in depth and horizontal range become

$$\Delta Z = - \frac{c_o}{G \cos A_o} (\cos A_o - \cos A) \qquad (37)$$

and

$$\Delta r = - \frac{c_o}{G \cos A_o} (\sin A - \sin A_o) , \qquad (38)$$

where Z is the increase in depth and r is the increase in range from the reference position, and A is the angle of depression of the raypath at this range and depth.

When ΔZ is known, the new angle A may be found by

$$A = \cos^{-1} \left[\cos A_o \left(\frac{G\Delta Z}{c_o} + 1\right)\right] \quad . \tag{39}$$

The time-of-flight along the raypath may be simplified to

$$\Delta t = \frac{-1}{G} \int_{A_o}^{A} \frac{dA}{\cos A} \quad , \tag{40}$$

which upon integration yields

$$\Delta t = \frac{1}{G} \ln\left[\left(\frac{\cos A}{1 + \sin A}\right)\left(\frac{1 + \sin A_o}{\cos A}\right)\right] \quad . \tag{41}$$

2. STUTRACK I Construction

STUTRACK I (App. A) is designed to allow the determination of a minimum amount of environmental information necessary for agreement with the NUTRACK III results. The program determines the tilt-corrected coordinates and the raypath entry angle into the array in the same manner as NUTRACK III, but uses Eq. 39 to calculate the exit angle A from the layer, Eq. 40 to calculate the horizontal range traversed, and the time-of-flight from Eq. 41. The thickness of the layer, ΔZ, is determined on a point-to-point basis from the depths from which the velocity profile was established.

The values Δr and ΔZ are accumulated and the original travel time T is decremented as in NUTRACK III until

$$TG \geq T + \varepsilon \quad ,$$

where

$$TG = \Sigma \Delta t \quad ,$$

and

$$\varepsilon = .0005 \text{ sec.}$$

This value of ε ensures an accuracy of $\Sigma \Delta Z$ and $\Sigma \Delta r$ within ±3 inches. If TG is within ε of T, the process stops and the X, Y, and Z coordinates for this isogradient technique (XG,YG,ZG) are calculated as in NUTRACK III,

$$XG = \frac{CORX}{H} \Sigma \Delta r \quad , \tag{42}$$

$$YG = \frac{CORY}{H} \Sigma \Delta r \quad , \tag{43}$$

and

$$ZG = \frac{CORZ}{H} \Sigma \Delta r \quad . \tag{44}$$

When

$$TG > T + \varepsilon \quad ,$$

the program returns to the previous layer and a bracket-and-halving process begins in ΔZ until the proper ΔZ is

found to satisfy the ε criterion in time. XG, YG, and ZG are then found by Eqs. 42, 43, and 44.

STUTRACK I is also designed to permit the utilization of the velocity-profile data in varying incremental step sizes to allow a determination of the effect of a varying amount of environmental data. For example, if velocimeter data is gathered in two-foot steps, an incremental step size (INC) of 1 would automatically set ΔZ = 2 ft, and an INC of 10 would set ΔZ = 20 ft. Consideration of the source depth must be made prior to the invocation of STUTRACK I in its present form, as the setting of too large an INC can create $\Sigma \Delta Z$ greater than the array depth of 585 feet, resulting in an error message.

STUTRACK I is also designed to analyze the data with the same isovelocity technique as NUTRACK III, but in varying incremental step sizes for comparison with the isogradient method. These output coordinates are XI, YI, and ZI.

The inputs into STUTRACK I are: velocity profile, increment size, tilt correction, time of day in hours, minutes and seconds, T_x, T_y, T_z, T_c, RBNX, RBNY, and RBNZ. The output is six histograms of the differences between the NUTRACK III, ray bent coordinates, and their respective values as determined by STUTRACK I using both the isogradient and isovelocity methods. These differences and the STUTRACK I values are also printed.

IV. EXPERIMENTAL RESULTS

A. VELOCITY PROFILE

Figures 7 and 8 illustrate that the velocity profiles for station 1 (taken at 1115 hrs) and station 6 (taken at 1315 hrs) are equivalent below 85 feet. (See Fig. 2 for station positions.) The data for station 6, represented by the "+"'s, shows the "afternoon effect" of solar heating. Both profiles increase in velocity with depth at a greater rate than would be caused by pressure alone, implying a similarly increasing temperature profile. The colder surface water was fresher, however, due to the heavy spring rainfall and runoff from the snow-capped mountain peaks.

B. AUTOTAPE DATA

The Range's microwave Autotape system was used to track the sound boat. Its precision was much less than expected so that comparison with Range data was not attempted at this time and will have to wait until the Autotape data is subjected to extensive analysis.

C. ANALYSIS OF NUTRACK III RESULTS

1. One-Way Transmission Loss

The one-way transmission loss (TL) is determined by an assumption of spherical spreading and the relationship

$$TL(dB) = 20 \text{ LOG } R + aR \quad , \qquad (45)$$

where

a = attenuation constant in sea water for 75-kHz sound,

≐ 0.03 dB/meter.

Figure 9 shows that at short ranges (station 1) the TL is dominated by the spherical spreading term. Beyond a "critical range" of approximately 1000 feet for 75-kHz sound, the losses due to absorption of sound in sea water will overpower the spreading and the transmission loss will increase rapidly at greater distances. The TL from station 6 to the hydrophone array is approximately 105 dB, but is only 57 dB from station 1.

2. RBNX, RBNY, RBNZ and Slant Ranges For Stations 1-25 and 6-50

Figures 10-13 show the 80 data for station 1-25 plotted versus time. Figures 14-16 represent the same data as Figs. 10-12 but with a linear drift correction. Figures 17-21 are similar curves for the 66 data for station 6-50, except that a drift correction was applied only to the slant range curve. These two stations were chosen for preliminary investigation since station 1 was closest to the array while station 6 was farthest away. The RBNX, RBNY, and Slant Range scales for each station are nearly equivalent, but RBNZ data are plotted in a 5/1 ratio, since station 6 was five times the slant range of station 1. In all cases, station 1 data

show good point-to-point continuity while station 6 data, except for Slant Range, are very erratic. Microstructure was examined as the cause of this variation using the procedure of Medwin [2], but was determined to be capable of producing a maximum fluctuation of only ±1 foot, or only a small fraction of the actual variation.

3. Transformation to Spherical Coordinates

A transformation from the orthogonal coordinates RBNX, RBNY, and RBNZ to a spherical system was achieved using the following relations,

$$R = (RBNX^2 + RBNY^2 + RBNZ^2)^{1/2} \quad , \tag{46}$$

$$\Phi = SIN^{-1}\left(\frac{RBNZ}{R}\right) \quad ,$$

and

$$\Theta = TAN^{-1}\left(\frac{RBNY}{RBNX}\right) \quad ,$$

where Φ is the angle of elevation looking from the array to the source, and Θ is an arbitrarily defined azimuthal angle. A graph of Φ versus Θ is a scatter diagram of the projection of the data onto the surface of a sphere of radius R.

Figures 22-29 are station 1-25 plots of Φ and Θ as calculated from:

a. Ray bent coordinates (Figs. 22-24),
b. Ray bent coordinates, amplified, and with linear drift correction (Figs. 25-27),
c. COR coordinates, amplified (Figs. 28 and 29).

Figures 22-24 show a consistent, nearly linear drift, with good point-to-point continuity. Figures 26 and 29 are identical, as should be the case since NUTRACK III assumed a laterally homogeneous medium, thereby keeping the ratio Y/X constant. Figures 25 and 28 show similar but not identical variations, which was also expected since the COR coordinates assumed a vertically homogeneous medium and the raybent coordinates consider the inhomogeneities.

Figures 30-32 are station 6-50 plots of Φ vs. time, θ vs. time, and Φ vs. θ, respectively, as calculated directly from the raybent coordinates, and plotted to the same scales as Figs. 25-27. The variations are approximately the same in magnitude as for the same plots at station 1-25. However the scatter diagram for station 1-25 transforms into a five-foot square patch on the surface of a sphere of radius 900 feet. At station 6-50 this uncertainty grows with the ratio of the radii to a patch twenty-five feet square.

4. Error Determination

An error determination was made from the data from Figs. 12, 14, 15, and 17-19 by subtracting each datum from the average value drift-corrected coordinate and dividing by R. Variations from the averages were found to be less than 5×10^{-6} with a standard deviation (σ) less than 10^{-3}. This latter is comparable with the theoretical error determination of section III-A-4 on the basis of an error in determining the arrival time which is independent of range.

D. COMPARISON OF NUTRACK III TO STUTRACK I

Comparison of STUTRACK I data in both the isogradient and isovelocity modes with the NUTRACK III raybent coordinates was achieved by the following relationships

$$DXG = RBNX - XG \tag{47}$$
$$DYG = RBNY - YG$$
$$DZG = RBNZ - ZG$$

and

$$DXI = RBNX - XI \tag{48}$$
$$DYI = RBNY - YI$$
$$DZI = RBNZ - ZI \quad .$$

Station 6-50 data (Figs. 36-38) are consistent with station 1-25 data (Figs. 33-35), but much more dramatic since it was taken at a much greater range. These graphs are plots of DX, DY, and DZ for both the isogradient and isovelocity cases as a function of incremental step size. They show that the STUTRACK I results are essentially equivalent to the NUTRACK III data when INC = 1. However as INC is increased, the isovelocity technique gives consistently poorer results while the isogradient method's results remain adequate as INC increases. In all cases the STUTRACK I coordinates followed the NUTRACK III raybent coordinates point-for-point, but were biased to one side. A few seconds of computer time was also saved as a result of the isogradient technique at a greater INC than for the

comparable calculations via the isovelocity method since fewer layers had to be examined to achieve the same, or better, results.

Figure 39 is a histogram of DXG, INC = 1, at station 6-50. Its Gaussian nature is characteristic of all the histograms of DX, DY, and DZ at every INC tested, at both stations.

V. CONCLUSIONS

A. NUTRACK III DATA

The large variations in RBNX, RBNY, and RBNZ compared to the smoothness of the Slant Range may be explained by an examination of Eqs. 3, 4, 5, and 15. The individual coordinates are dependent upon the difference of T_c and T_x, T_y, or T_z. Since this difference is small, a small error in time will make a large fractional error in the computed coordinate. The uncertainty in signal discrimination, addressed in section III-A-4 and estimated as 3.3×10^{-6} sec, becomes important, causing significant random errors from pulse-to-pulse. This error becomes very large for any position for which the wave arrives at the two hydrophones at nearly the same time. For calculation of the Slant Range the arrival time is used alone so the fractional error is much less.

B. COMPARISON OF STATION 1-25 TO 6-50

Comparison of station 1-25 data to that from 6-50 shows the latter to have greater spatial variability. The transformation to spherical coordinates shows this difference is not present in the angular display. This is what would be expected if the time errors were the important sources of variability. This conclusion is upheld by an experimental error determination at both stations that agrees with the theoretical error induced by the one-fourth period

uncertainty in the signal arrival times. Out to the greatest distances studied (over twice that used in normal Range operations), the precision in measuring arrival times is unchanged even though the signal-to-noise ratio decreases by nearly 50 dB. Therefore, it is concluded that for conditions similar to those prevailing at the time of this experiment any attempt to improve the signal-to-noise level by increasing the source level will be nonproductive and wasteful. Improved Range accuracy can only be obtained by improving the accuracy of the time measurements (above its present value of about one-quarter period of the 75-kHz signal) or increasing the baseline of the hydrophone array.

C. EFFECT OF ENVIRONMENTAL DATA

The graphs of DX, DY, and DZ for both stations show conclusively that for the conditions prevailing at the time of this experiment the isogradient technique of STUTRACK I provides better results with less environmental data than does NUTRACK III. This is consistent in each of the plots but is explicit in DZ at station 6, where the isovelocity layer method results in a linear growth in DZ as the incremental step size (INC) is increased, but little change in DZ in the isogradient technique. Conclusive in this is that much less environmental data need be collected if a isogradient program were used.

VI. COMMENTS AND RECOMMENDATIONS

This thesis treated the NUTRACK III data as a comparator for analysis for both modes of STUTRACK I, but no conclusive evidence has been gathered to determine which is more accurate. The Range's Autotape system was to have determined this, but was so imprecise that a decision was unreachable without detailed analysis of the Autotape results.

In all Z calculations at both stations the source depth plus Z was less than the array depth by three-to-ten feet. No hypothesis has been reached for the cause of the disappearance of these few feet.

Further study of the data is needed to determine if the results from the intermediate stations are consistent with the conclusions reached here. Then, these conclusions should be tested using sound-velocity profiles representing other Dabob Bay oceanographic conditions. Special consideration should be given to the apparent inaccuracy in Z.

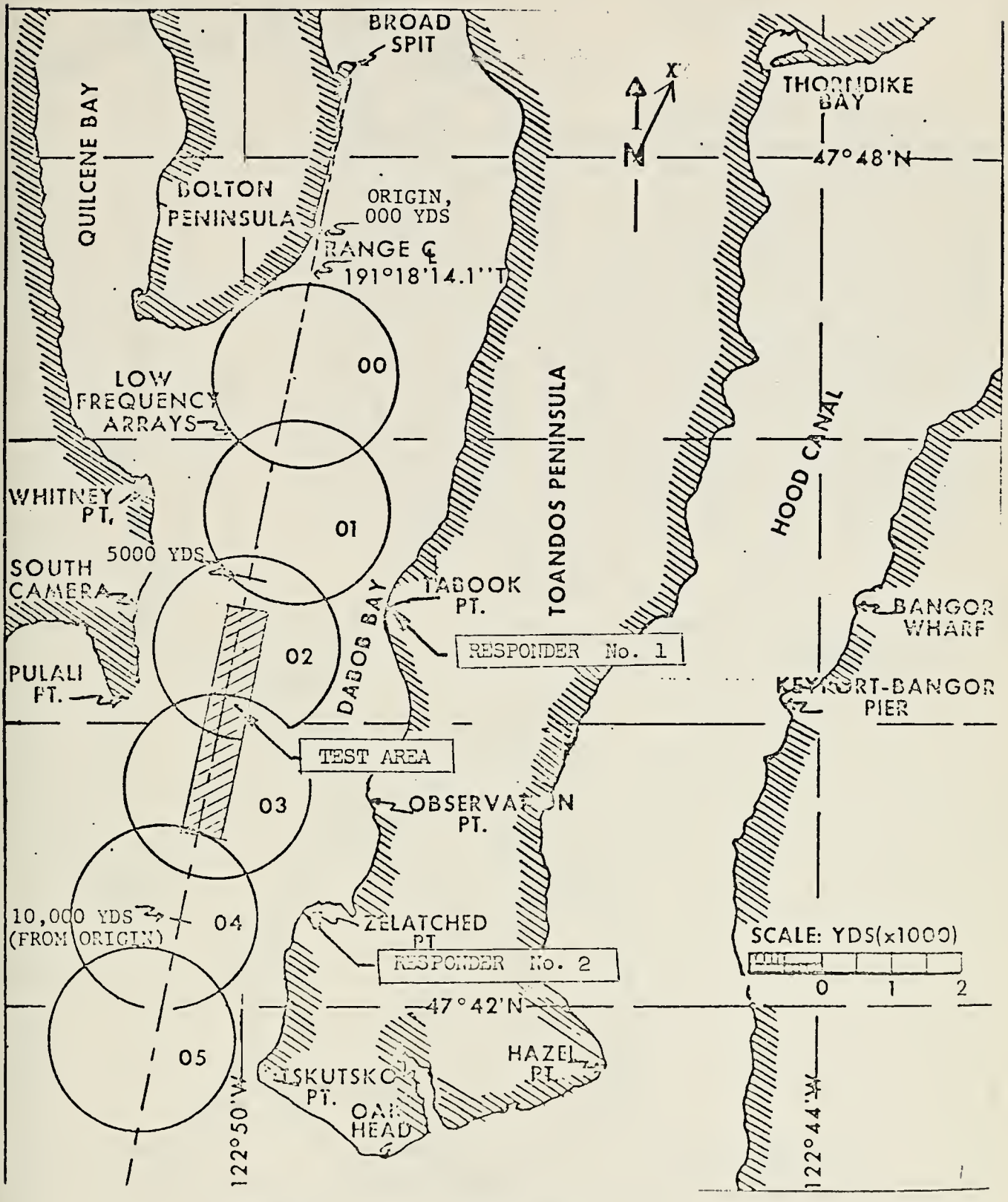

FIGURE 1. DABOB BAY RANGE

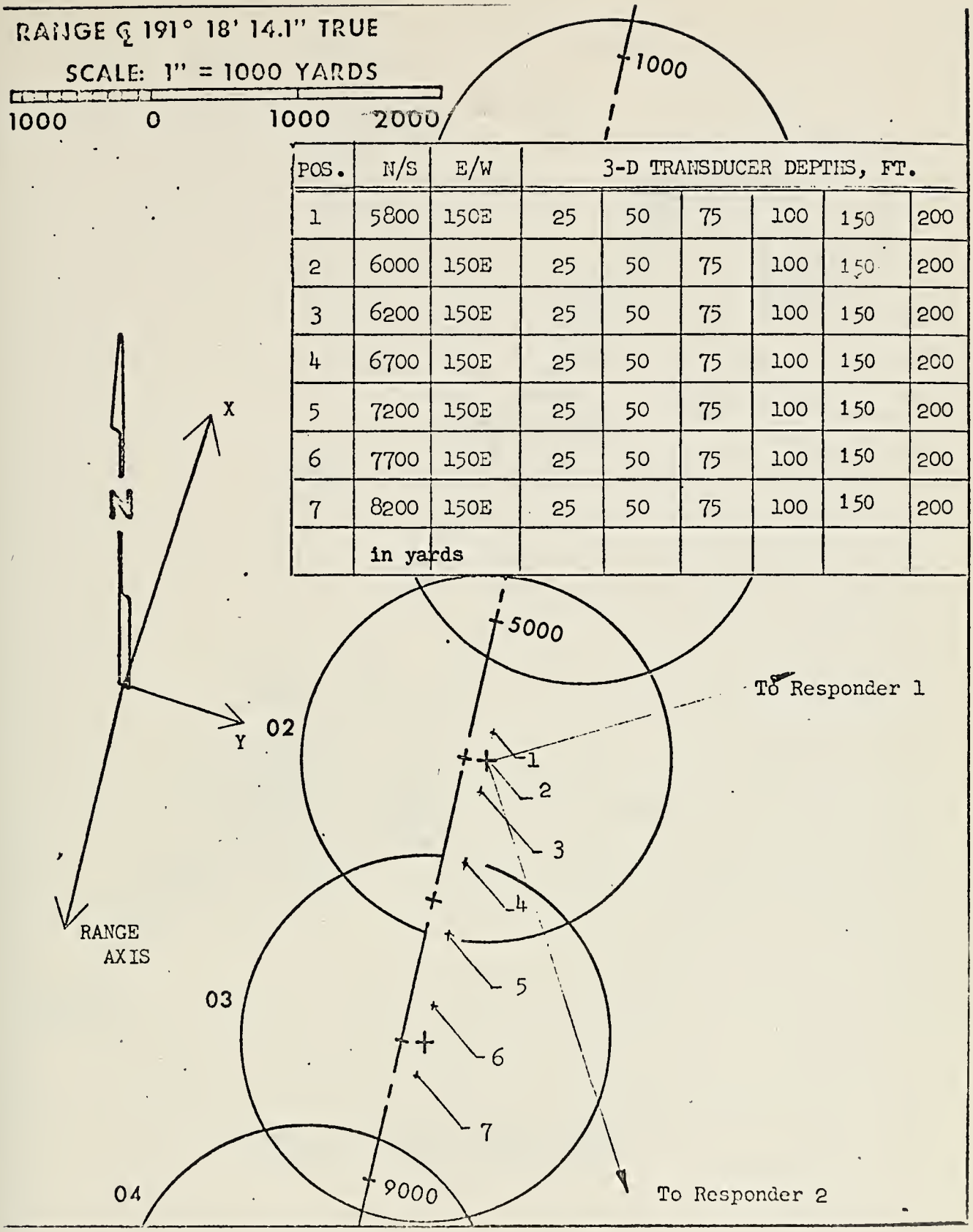

POS.	N/S	E/W	3-D TRANSDUCER DEPTHS, FT.					
1	5800	150E	25	50	75	100	150	200
2	6000	150E	25	50	75	100	150	200
3	6200	150E	25	50	75	100	150	200
4	6700	150E	25	50	75	100	150	200
5	7200	150E	25	50	75	100	150	200
6	7700	150E	25	50	75	100	150	200
7	8200	150E	25	50	75	100	150	200
	in yards							

FIGURE 2. EXPERIMENTAL AREA

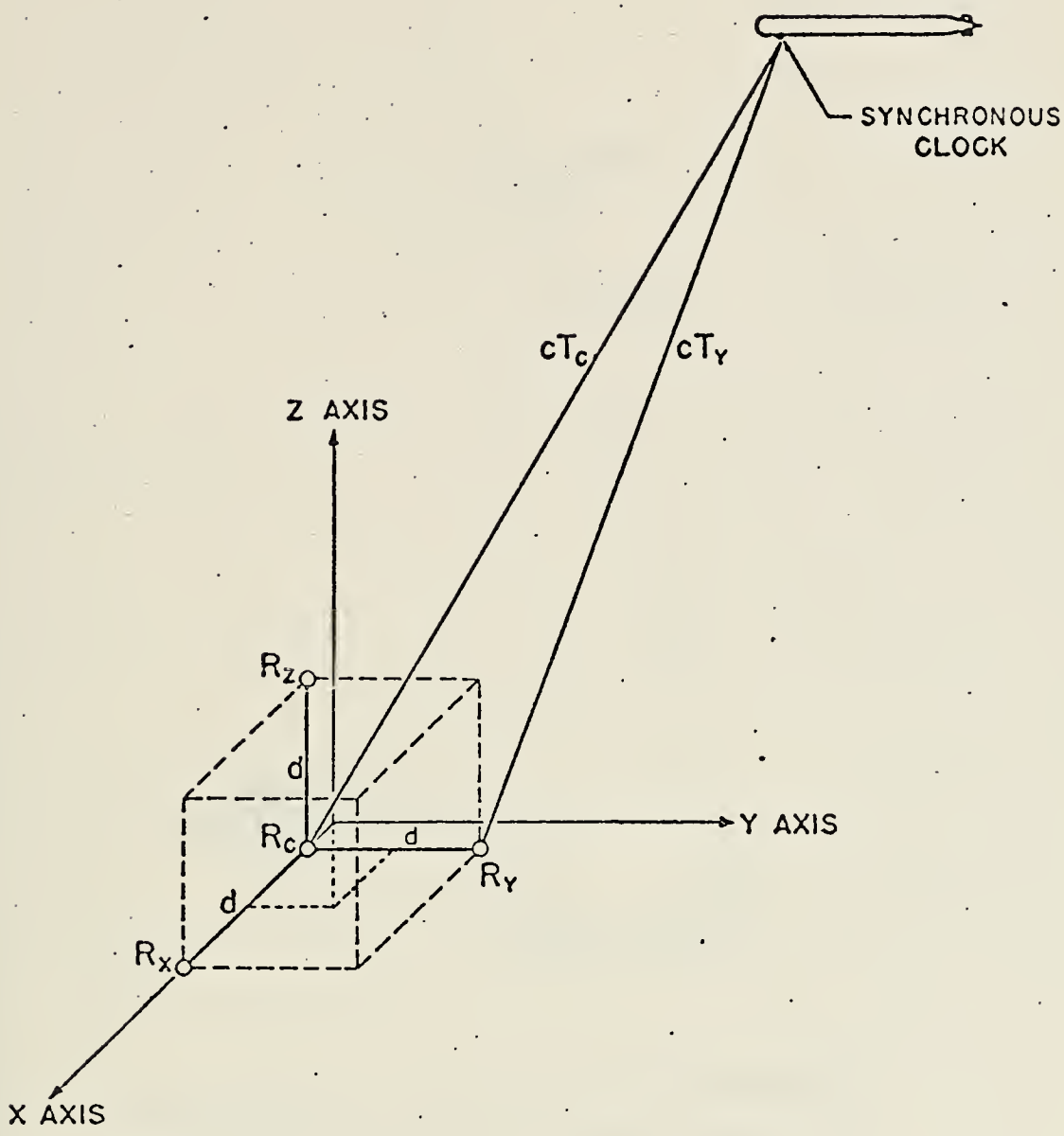

FIGURE 3. HYDROPHONE ARRAY

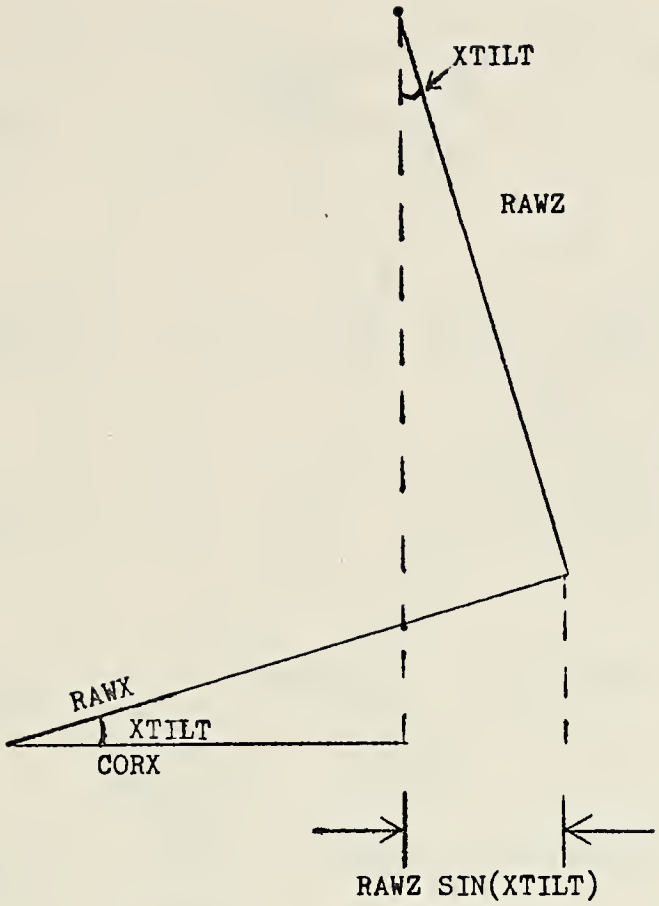

The SIN(XTILT) is positive when the X transducer is above the horizontal plane passing through the C transducer, and negative when the X transducer is below the horizontal plane passing through C.

FIGURE 4. TILT CORRECTION

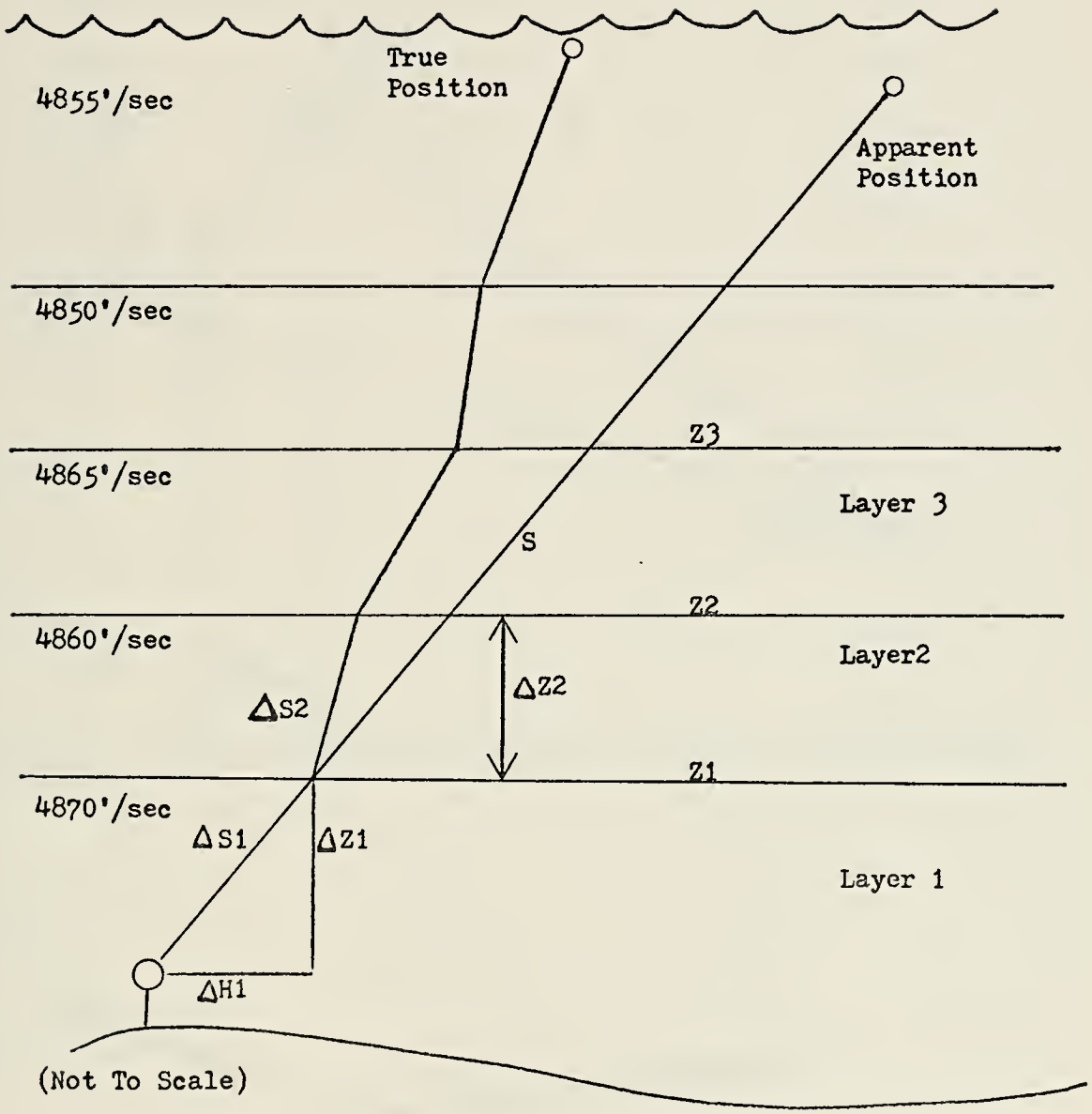

FIGURE 5. RAY PATH REFRACTION

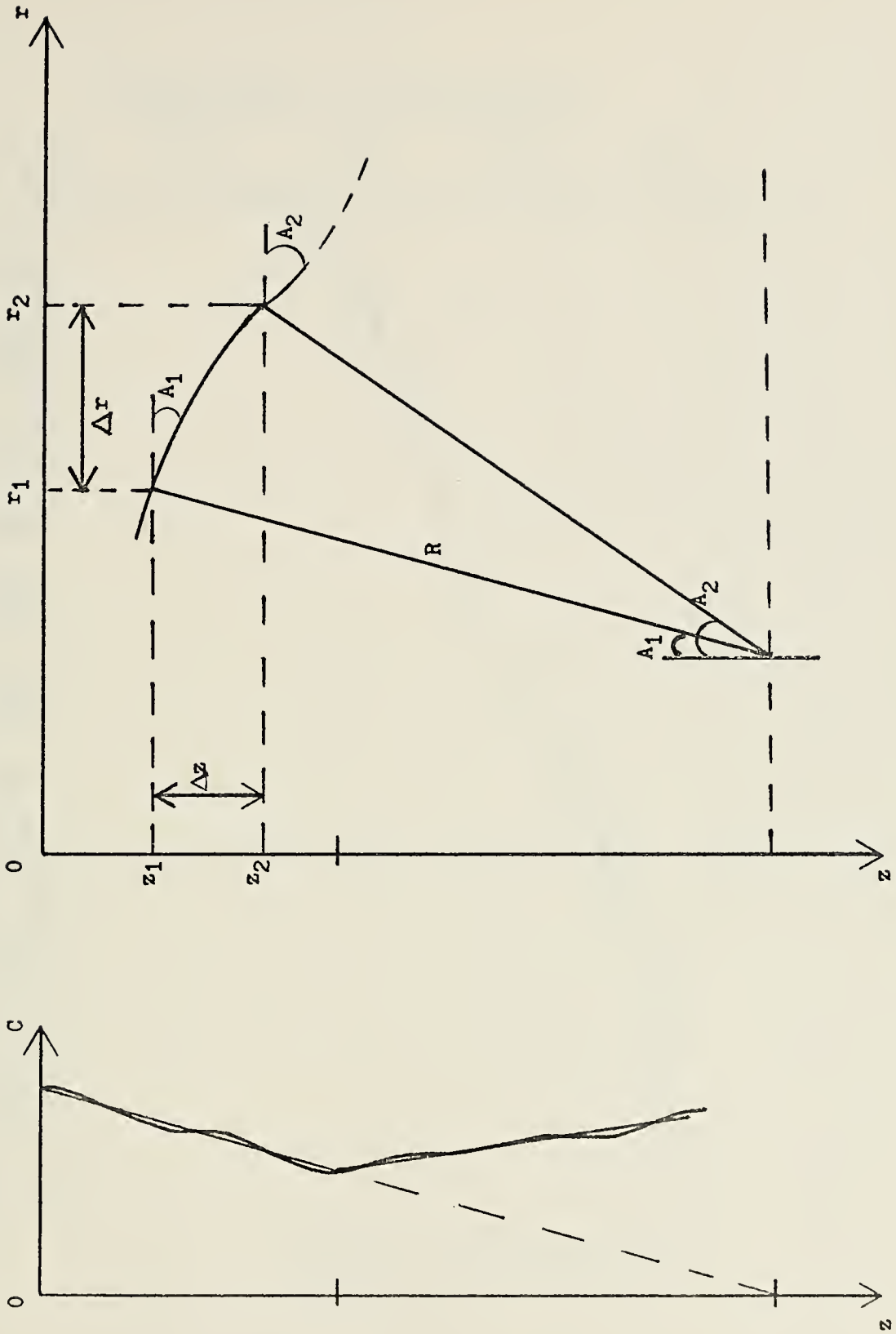

FIGURE 6. ISOGRADIENT THEORY

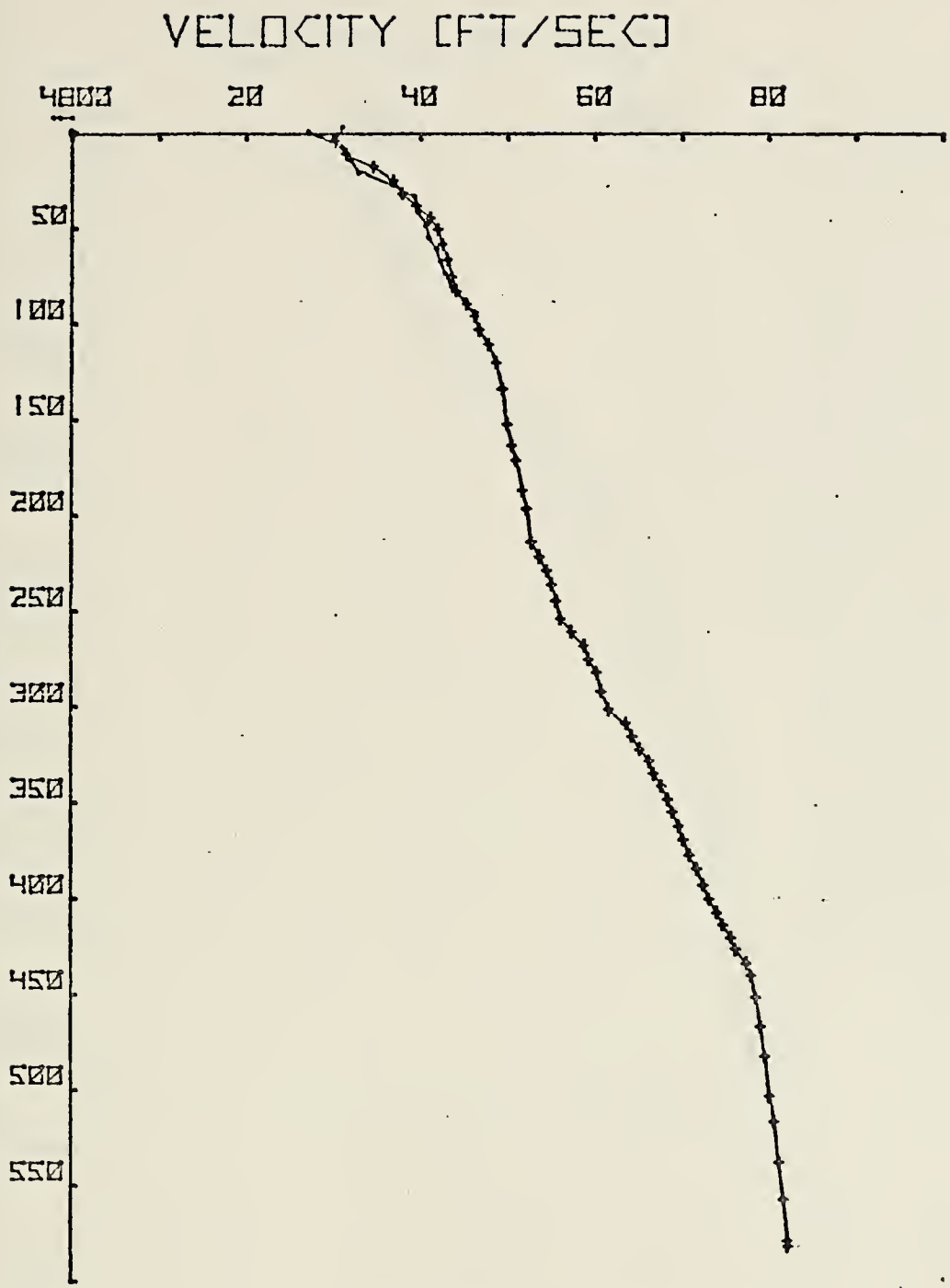

FIGURE 7. VELOCITY PROFILE

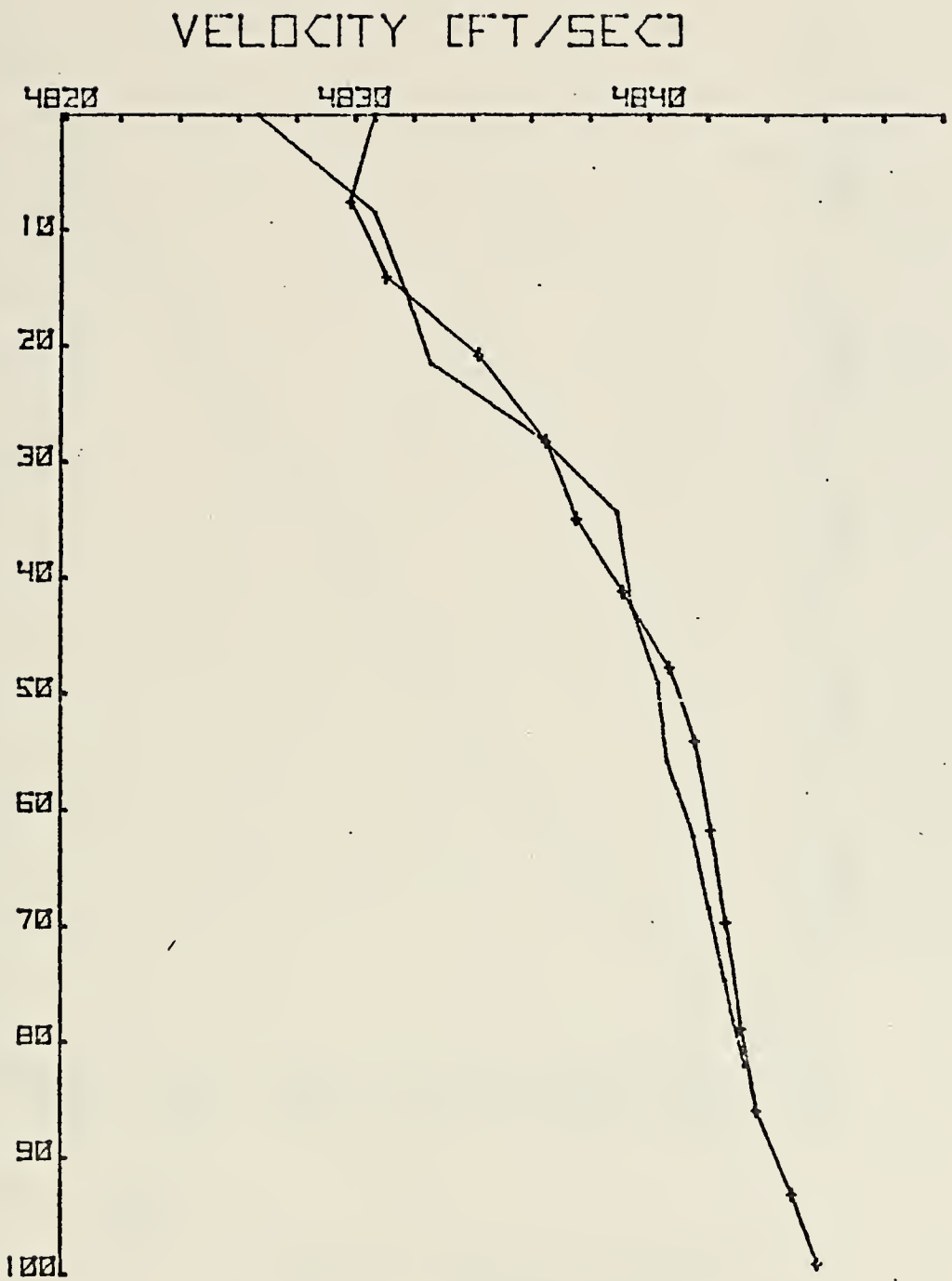

FIGURE 8. VELOCITY PROFILE

FIGURE 9. TRANSMISSION LOSS

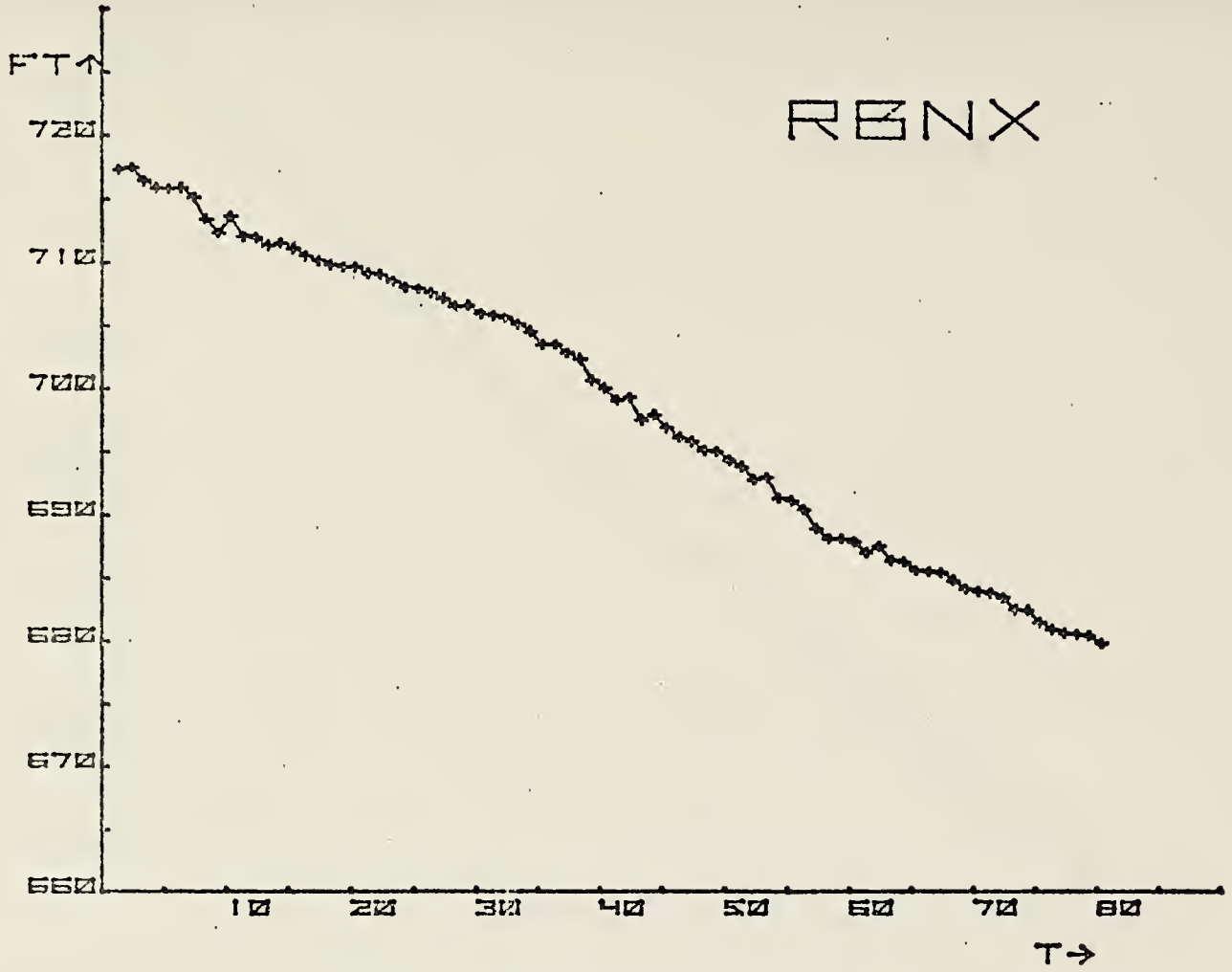

FIGURE 10. RBNX, Station 1-25

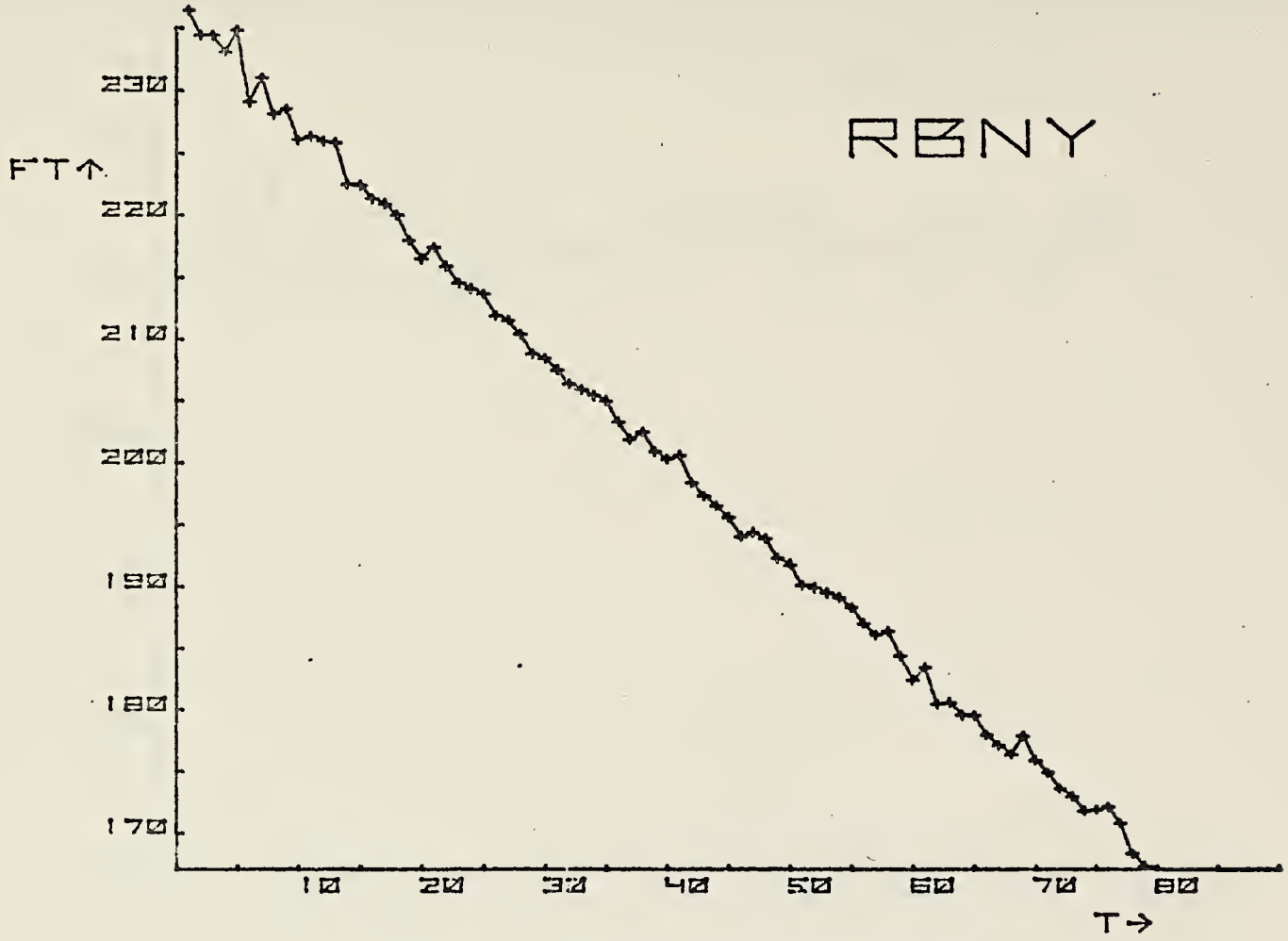

FIGURE 11. RBNY, Station 1-25

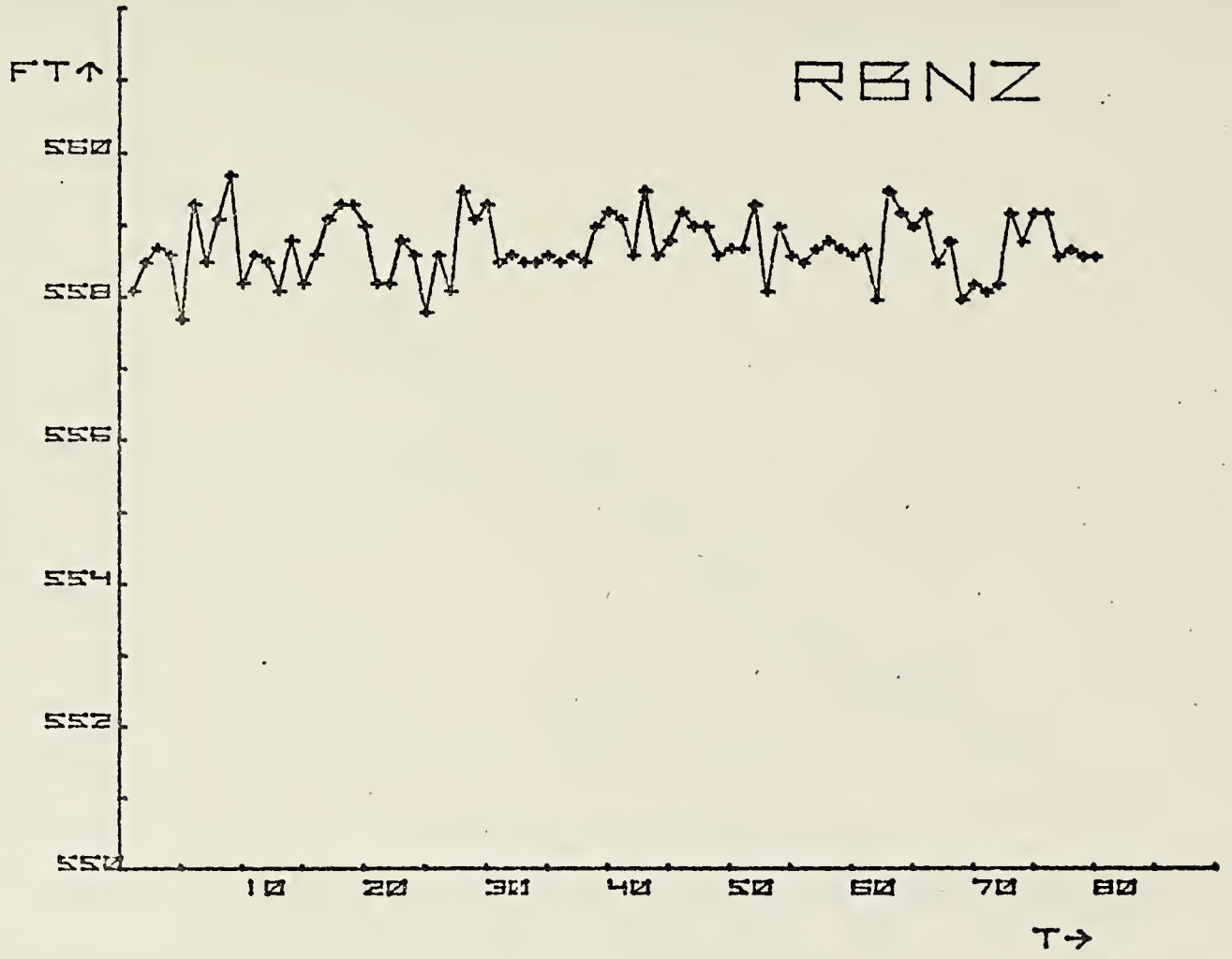

FIGURE 12. RBNZ, Station 1-25

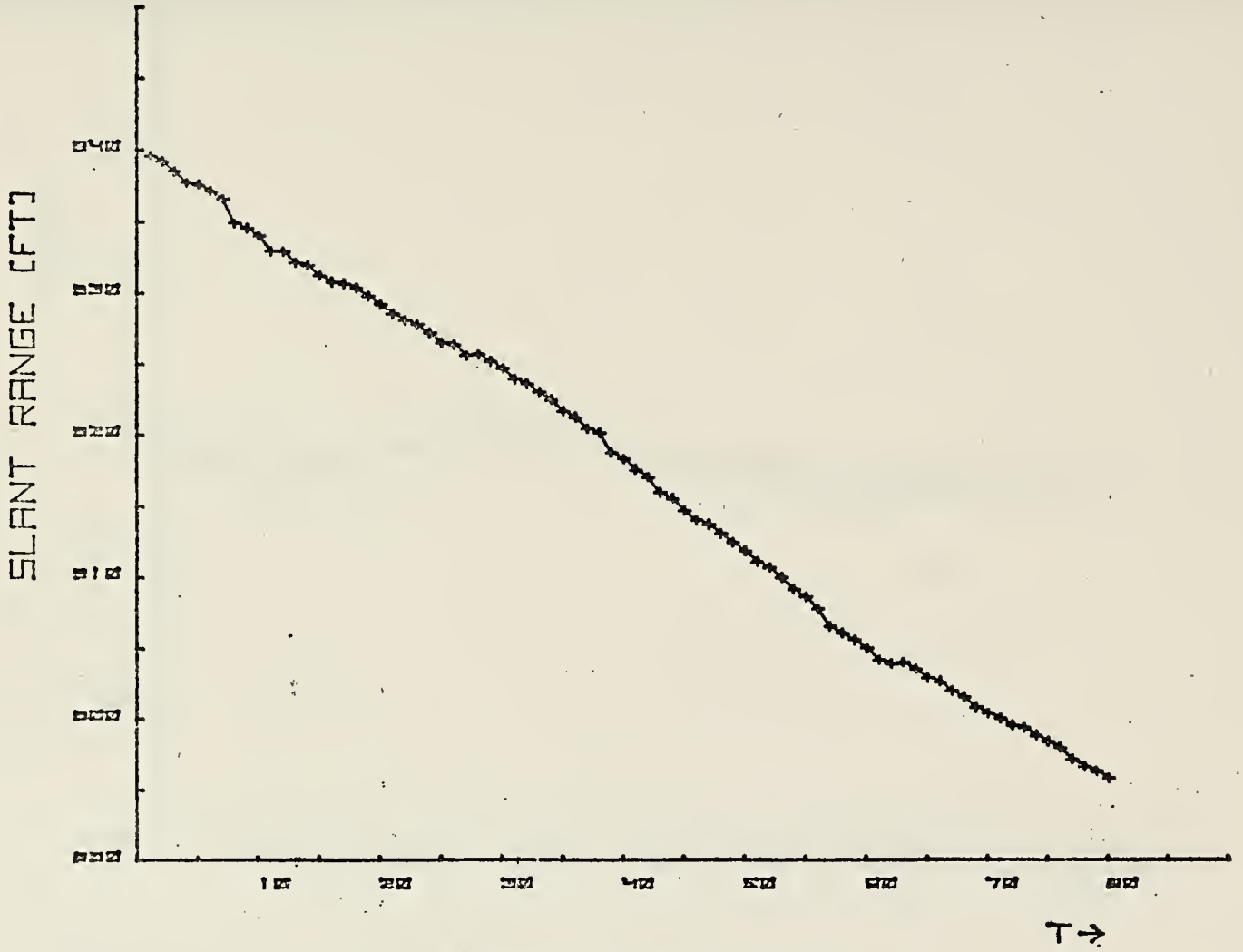

FIGURE 13. SLANT RANGE, Station 1-25

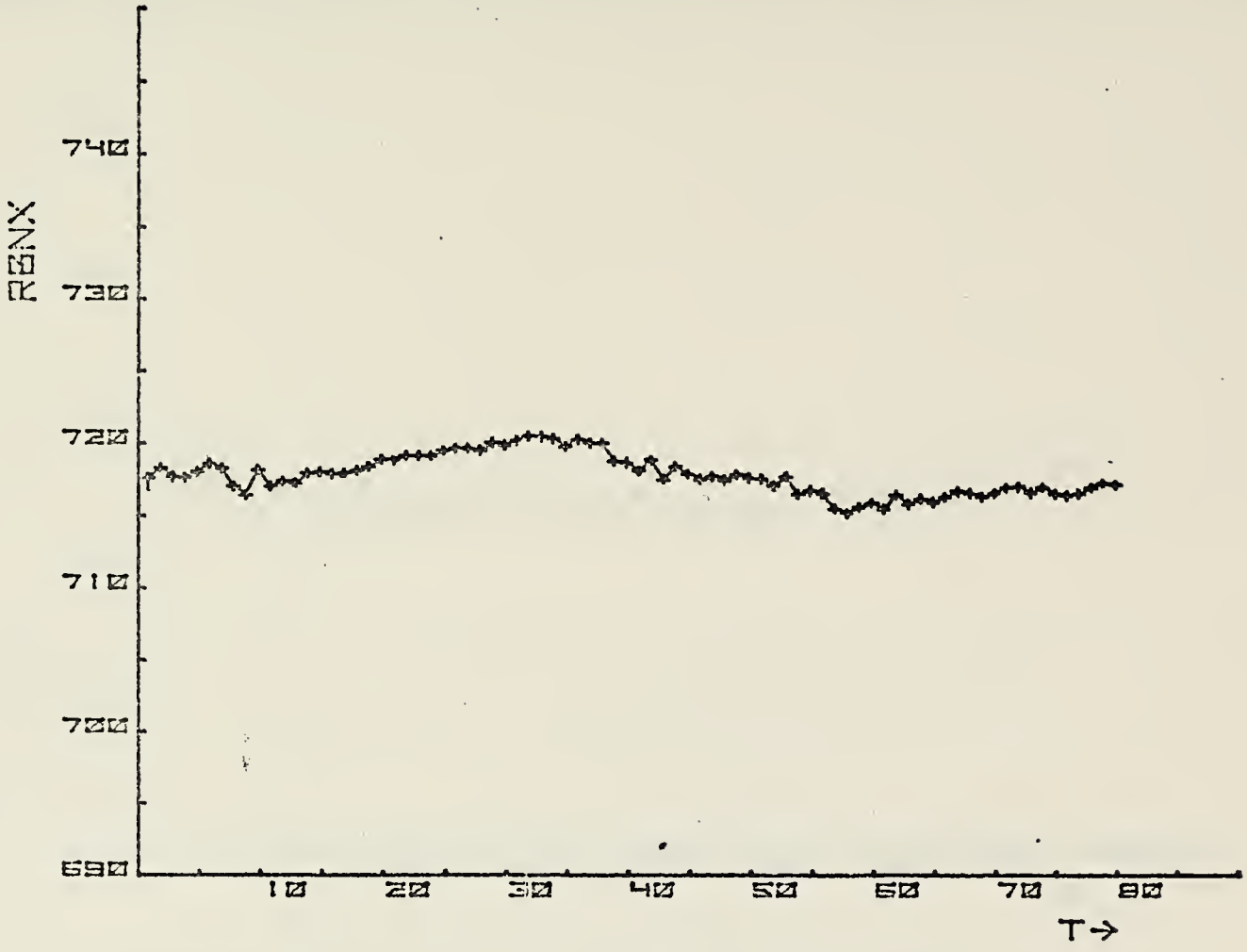

FIGURE 14. RBNX, DRIFT CORRECTED, Station 1-25

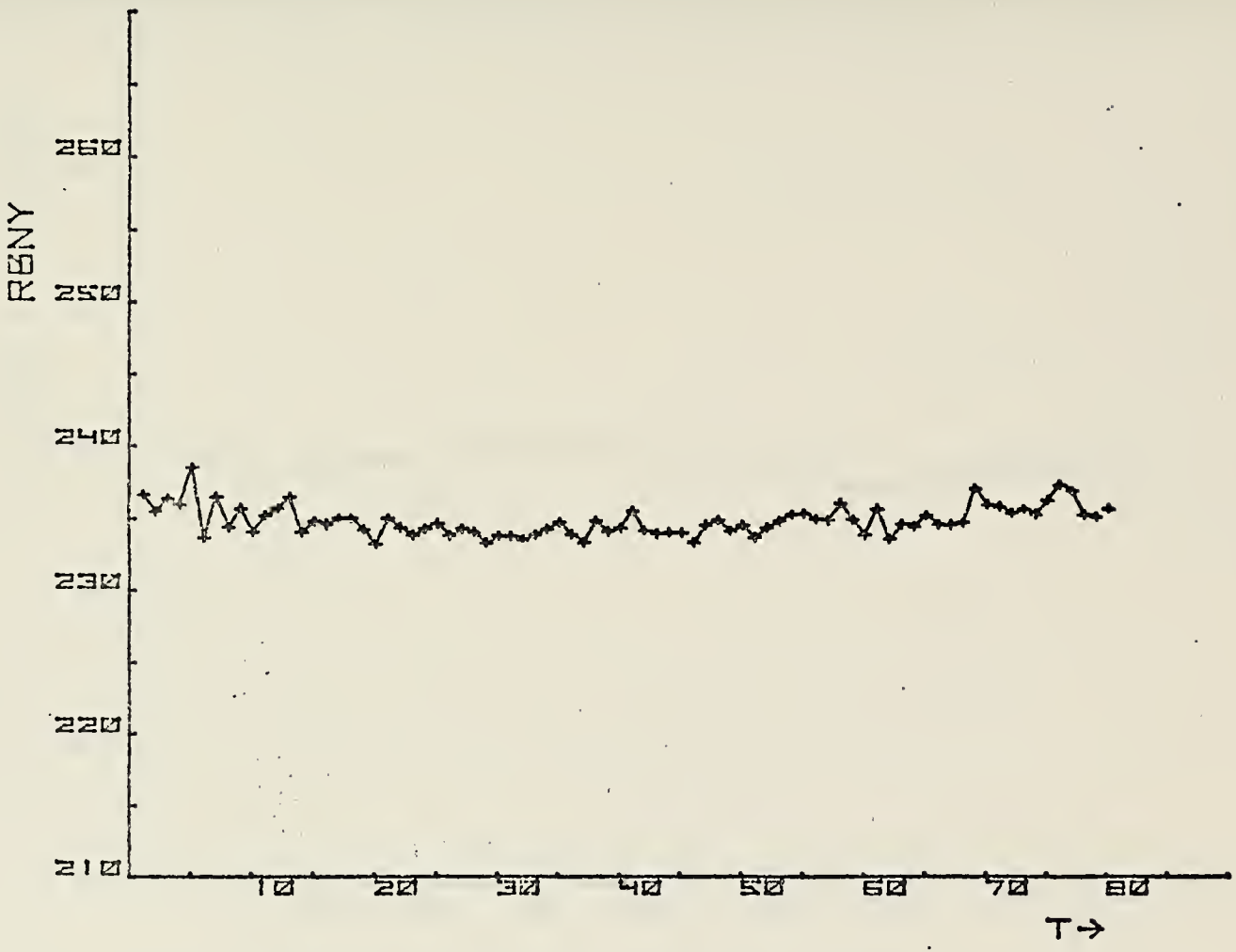

FIGURE 15. RBNY, DRIFT CORRECTED, Station 1-25

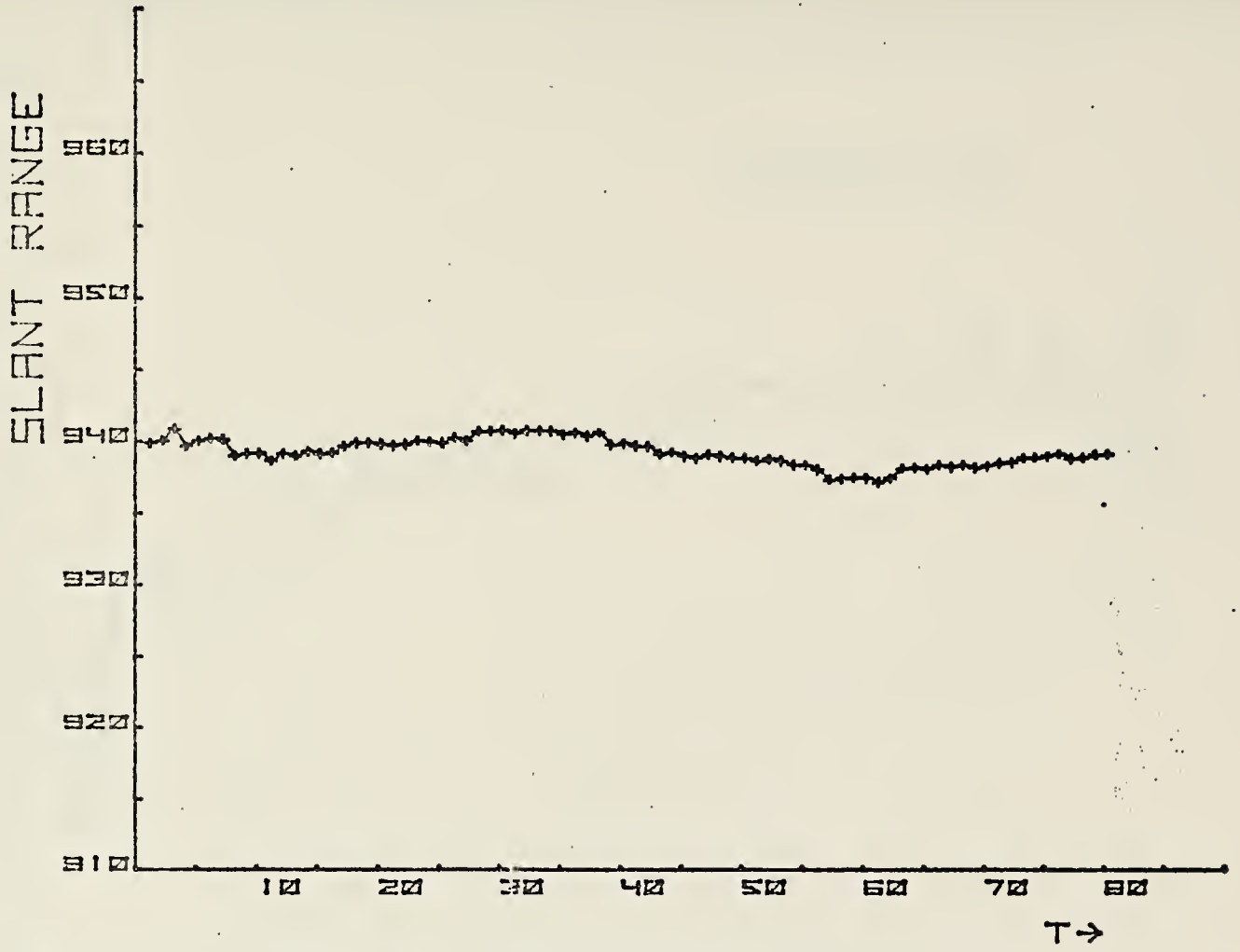

FIGURE 16. SLANT RANGE, DRIFT CORRECTED, Station 1-25

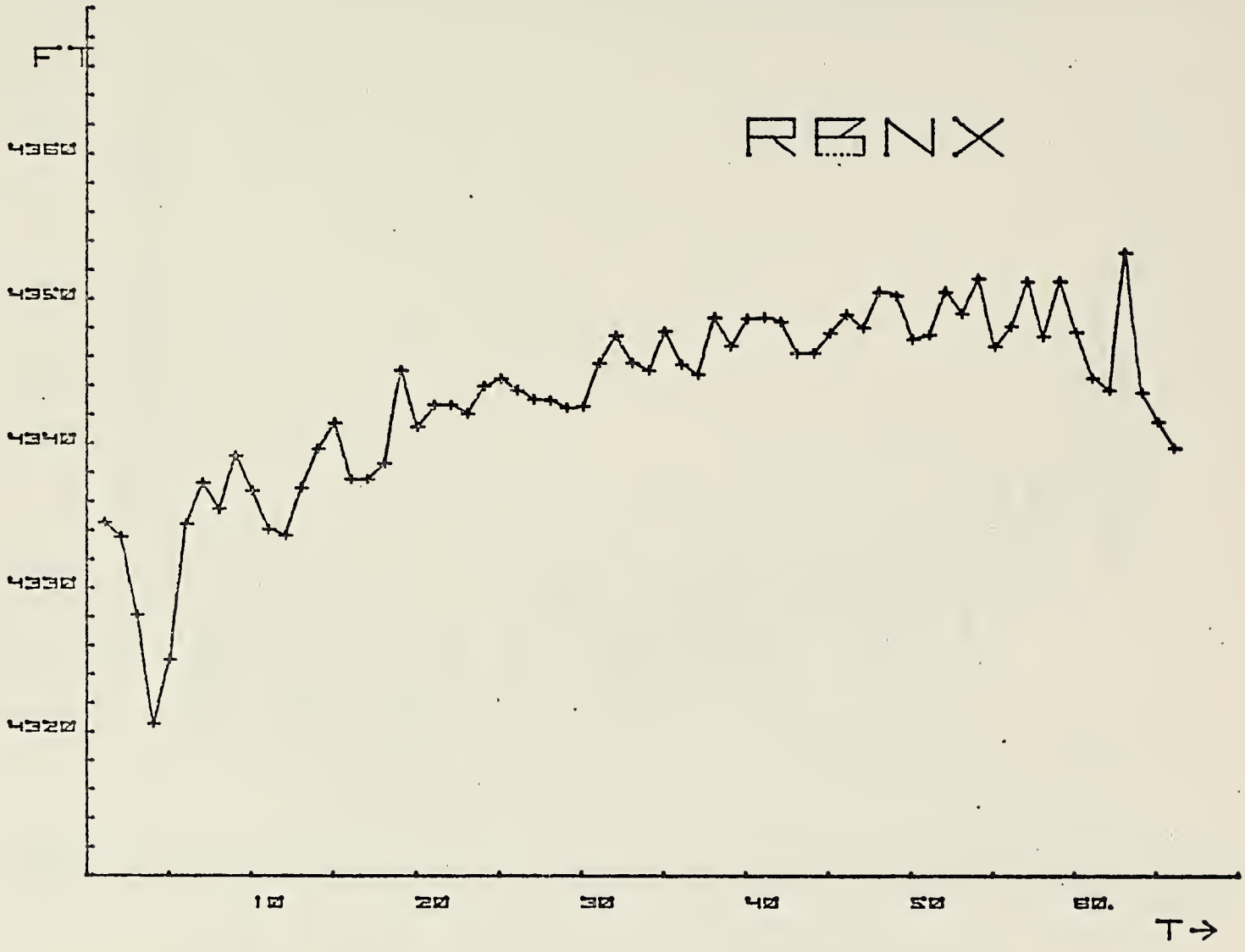

FIGURE 17. RBNX, Station 6-50

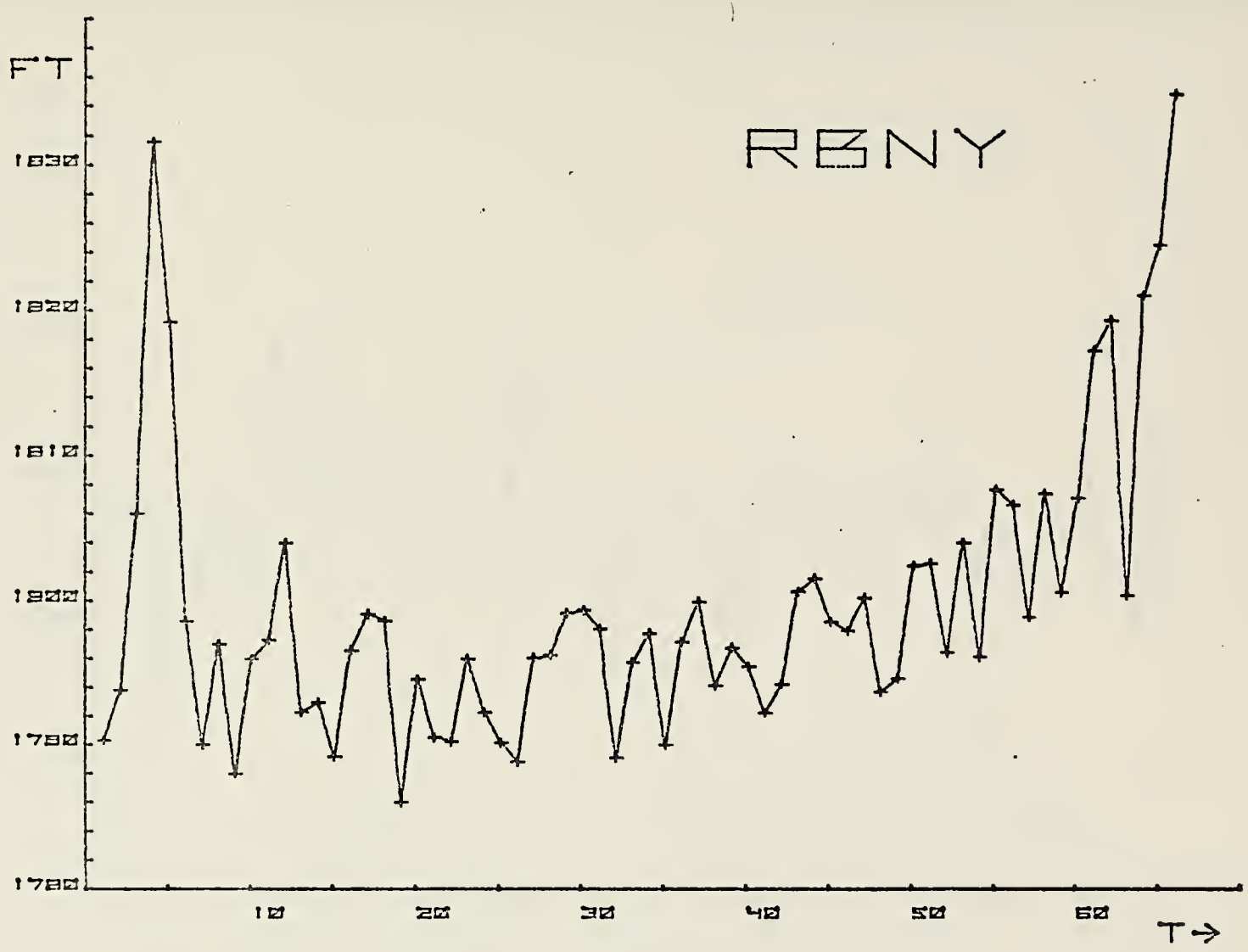

FIGURE 18. RBNY, Station 6-50

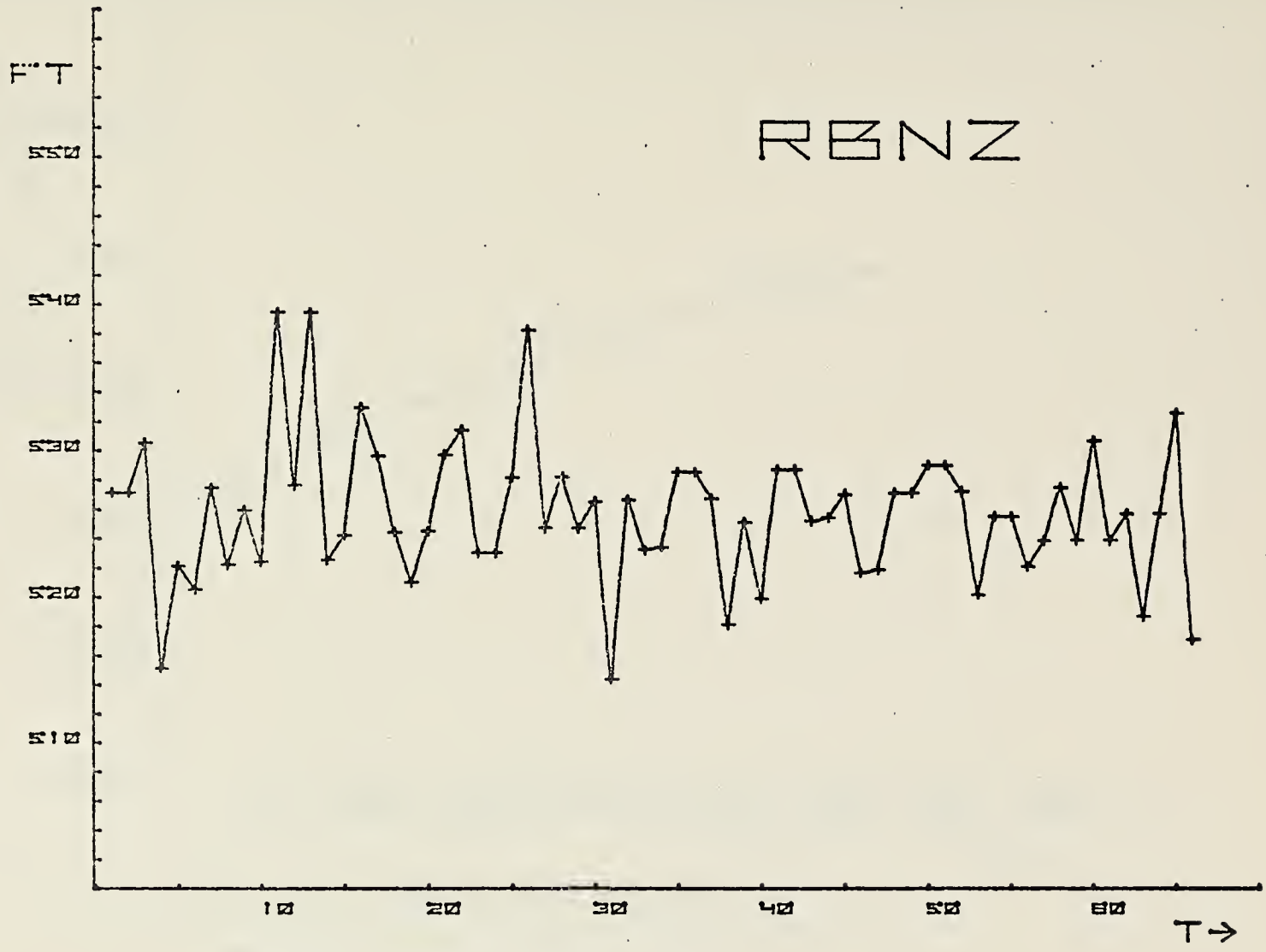

FIGURE 19. RBNZ, Station 6-50

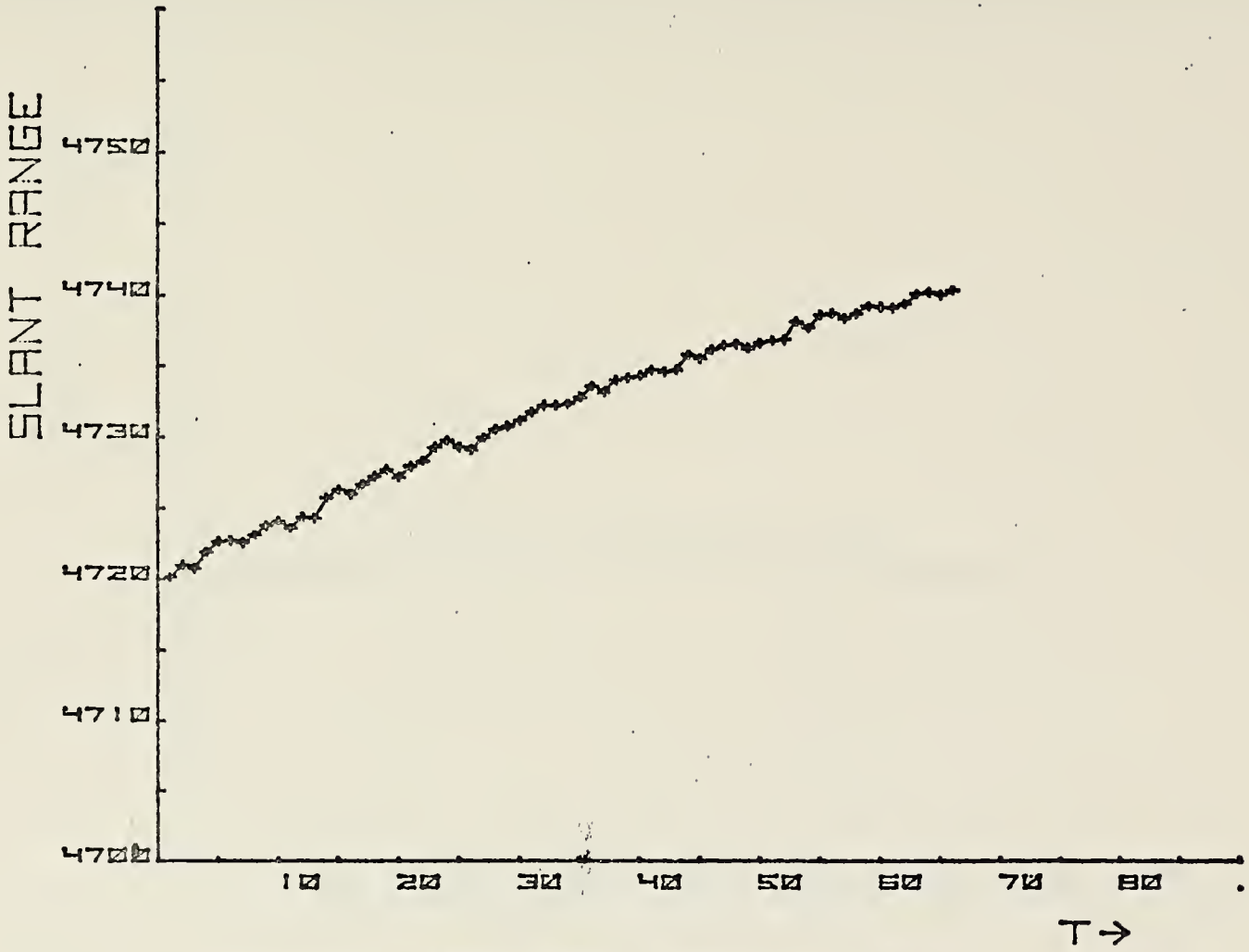

FIGURE 20. SLANT RANGE, Station 6-50

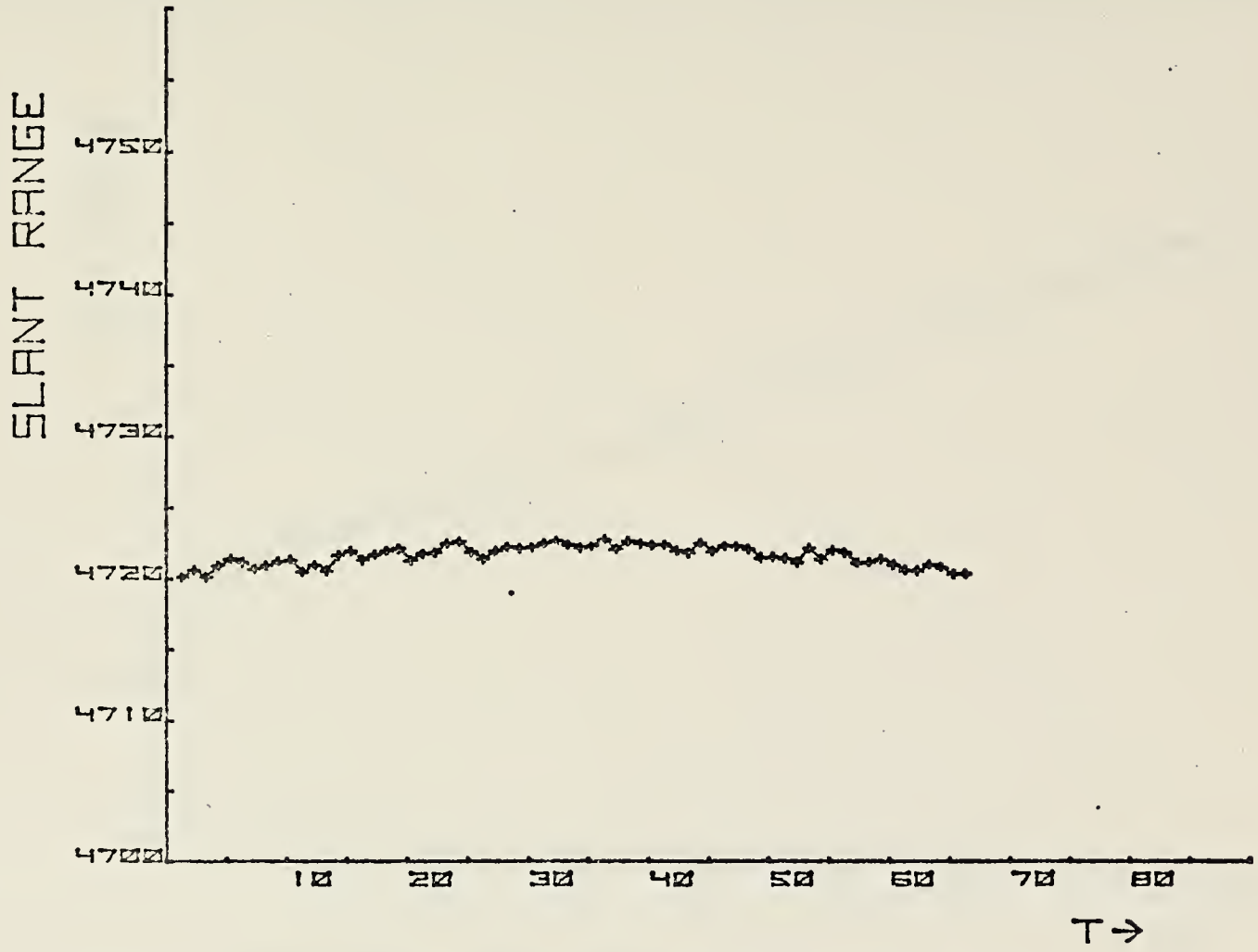

FIGURE 21. SLANT RANGE, DRIFT CORRECTED, Station 6-50

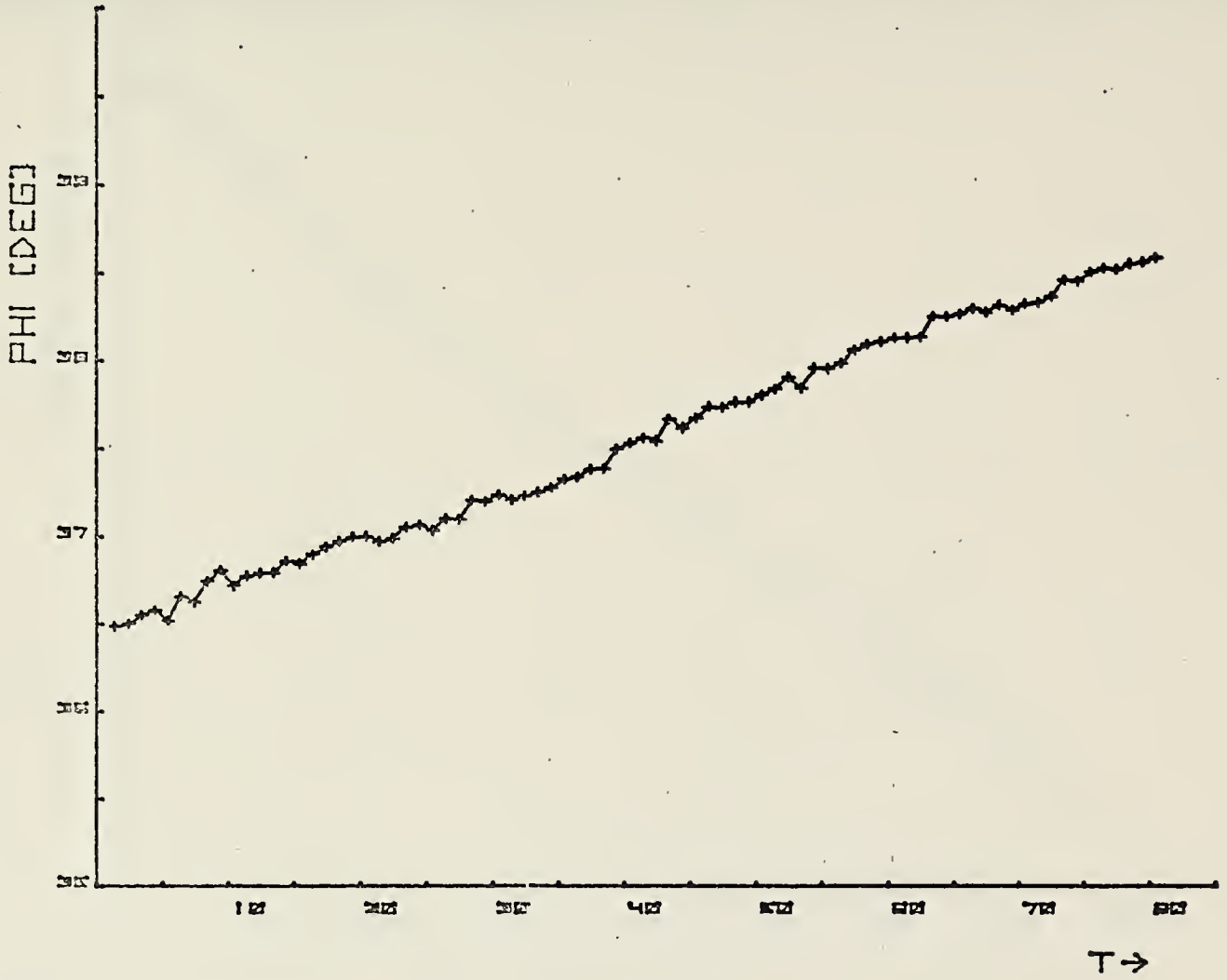

FIGURE 22. PHI, Station 1-25

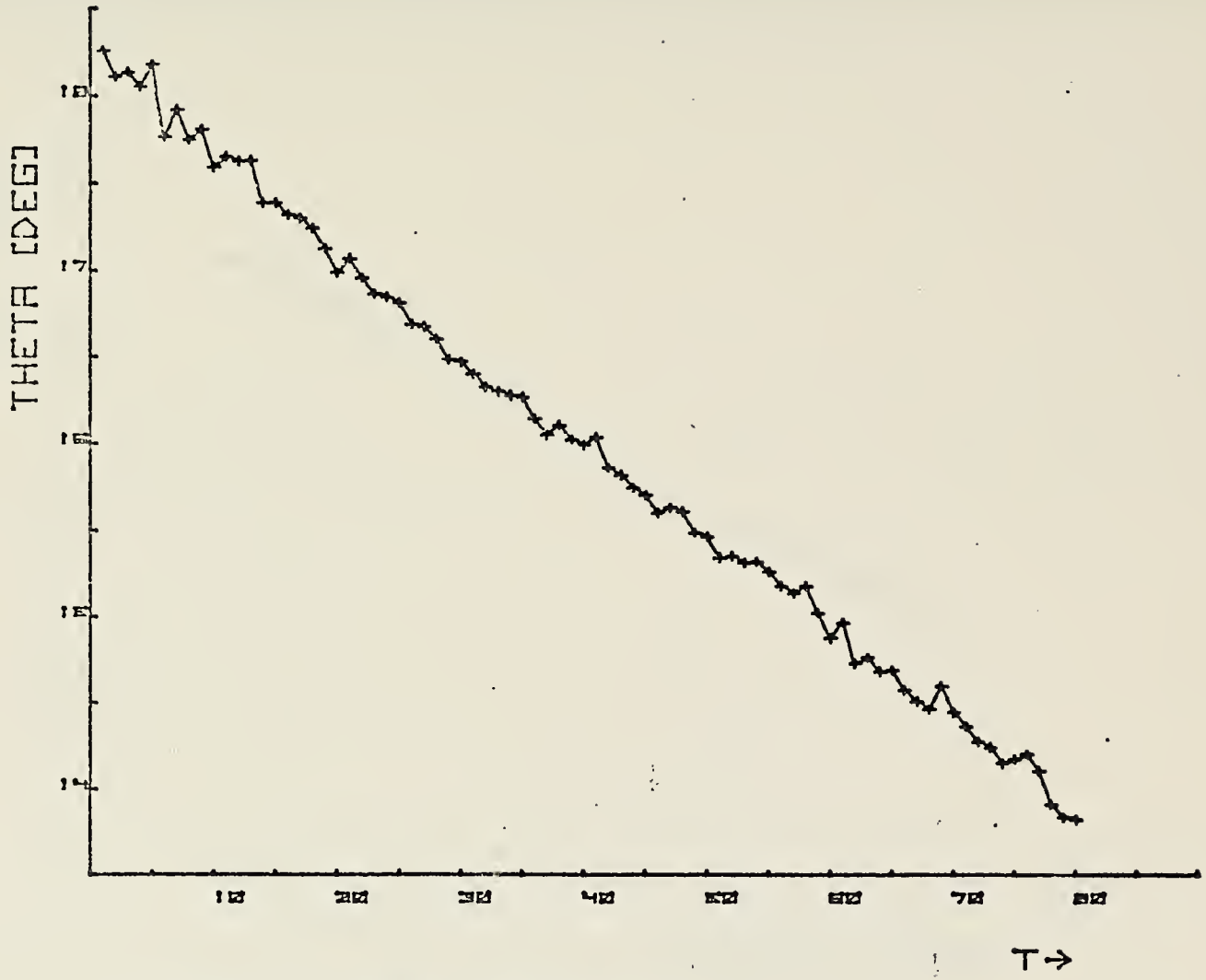

FIGURE 23. THETA, Station 1-25

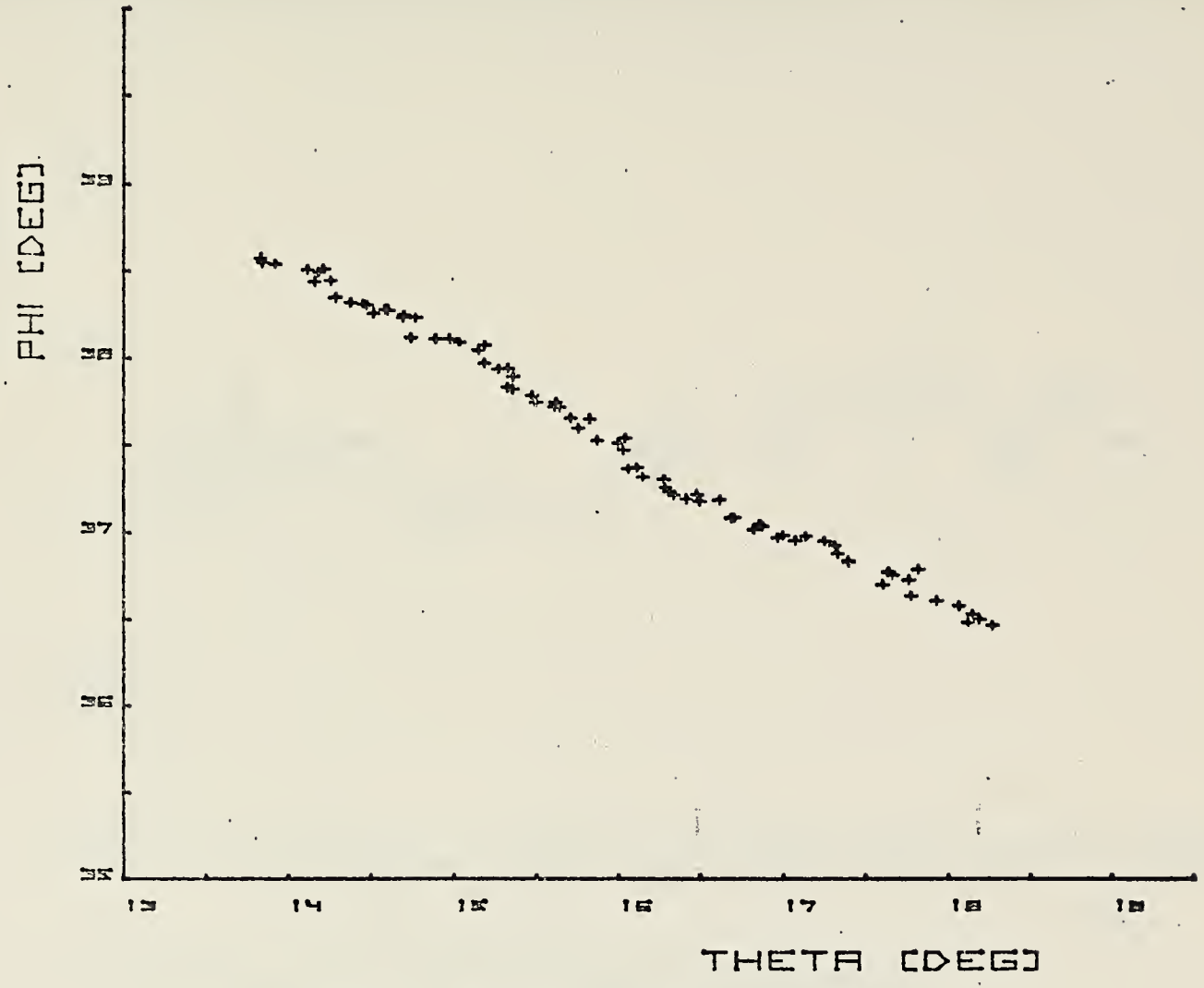

FIGURE 24. PHI vs. THETA, Station 1-25

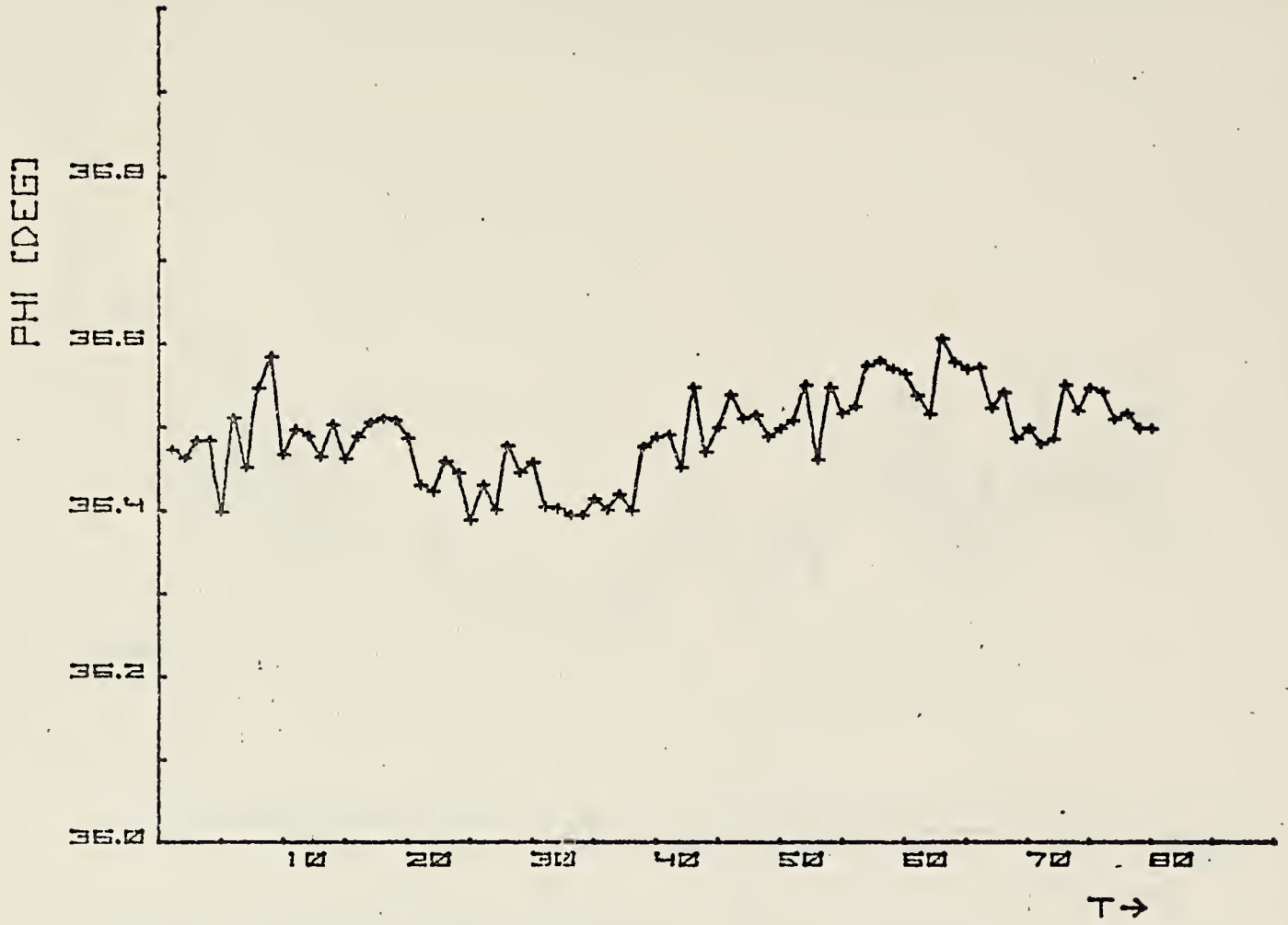

FIGURE 25. PHI, DRIFT CORRECTED, Station 1-25

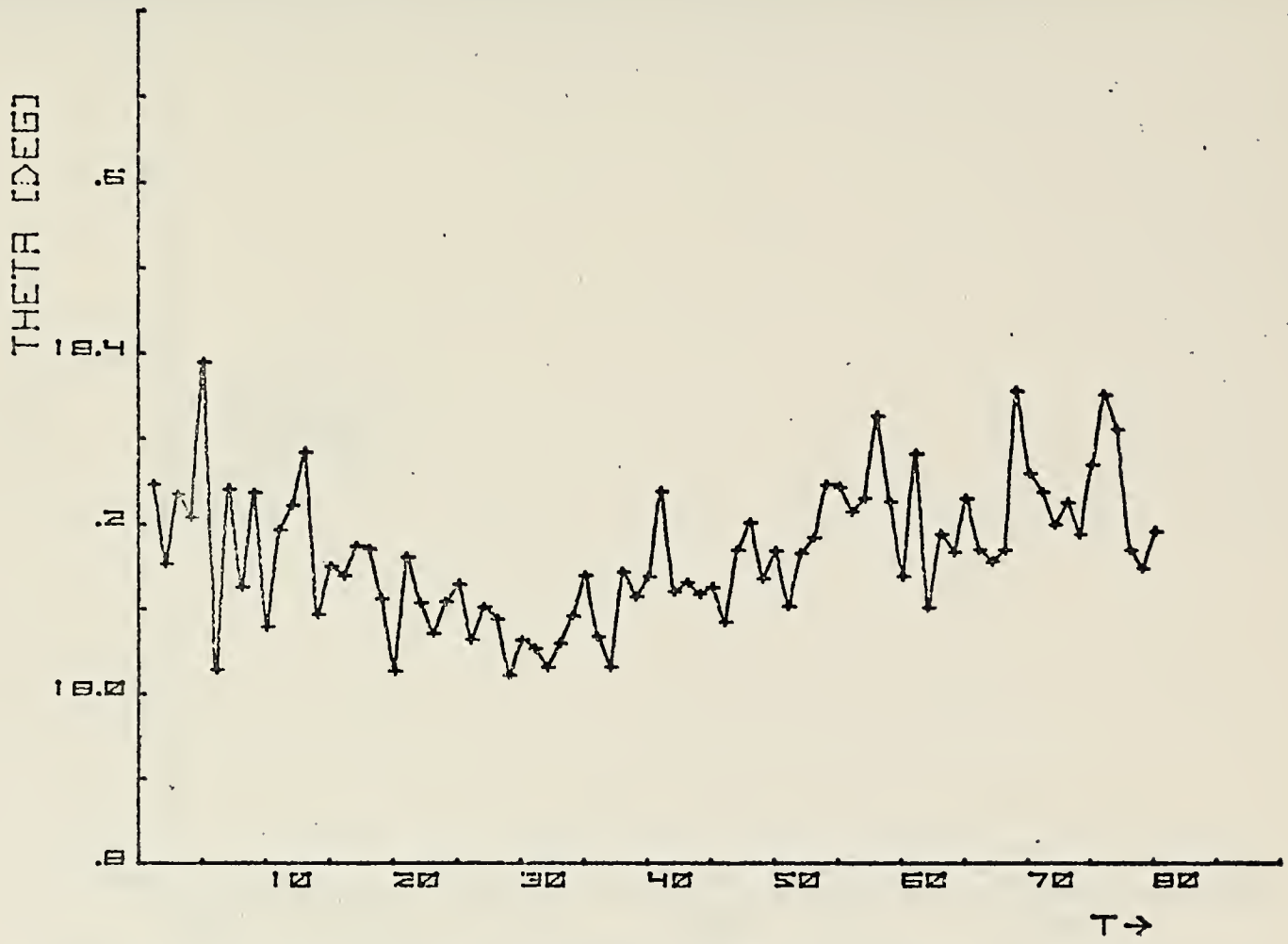

FIGURE 26. THETA, DRIFT CORRECTED, Station 1-25

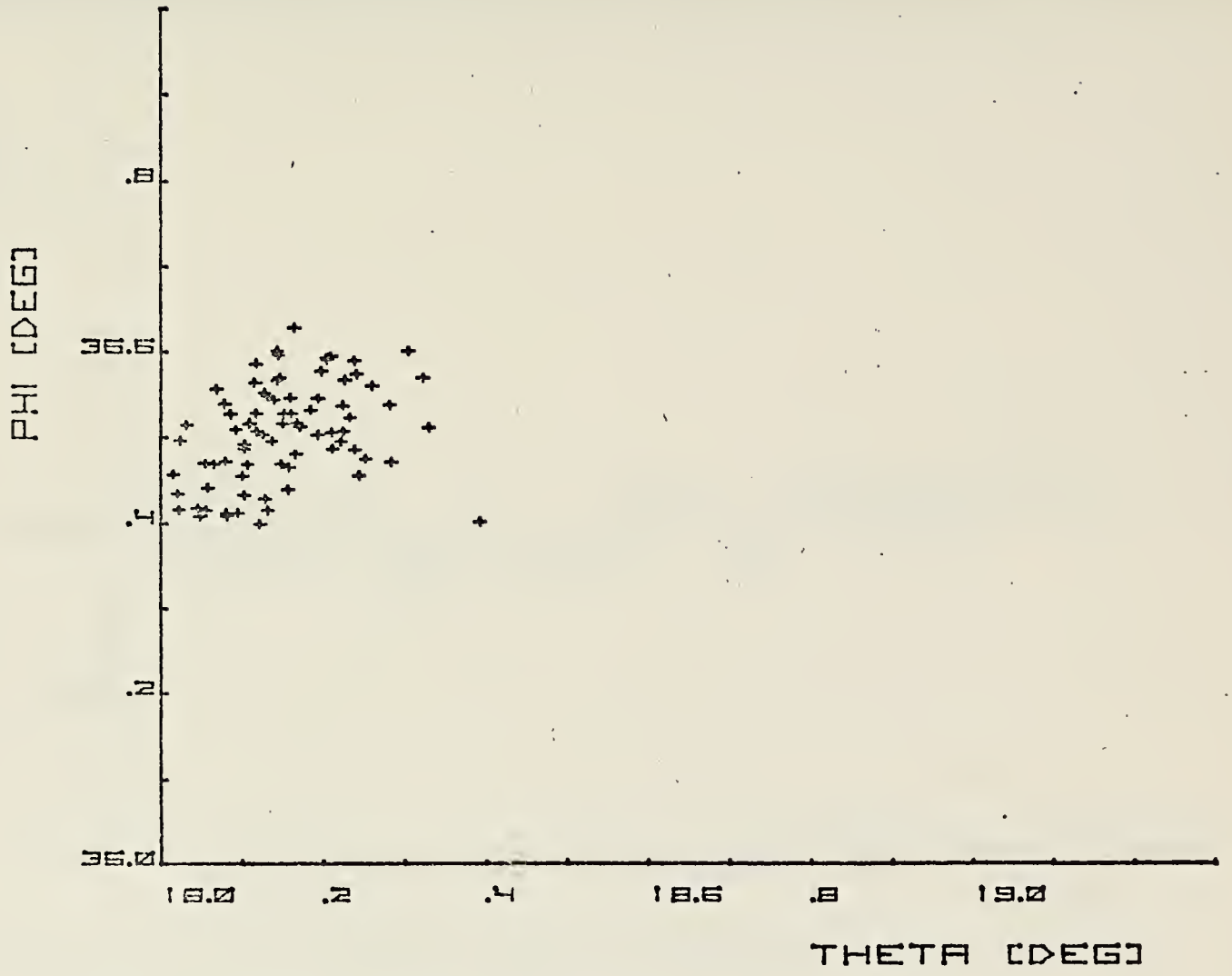

FIGURE 27. PHI vs. THETA, DRIFT CORRECTED, Station 1-25

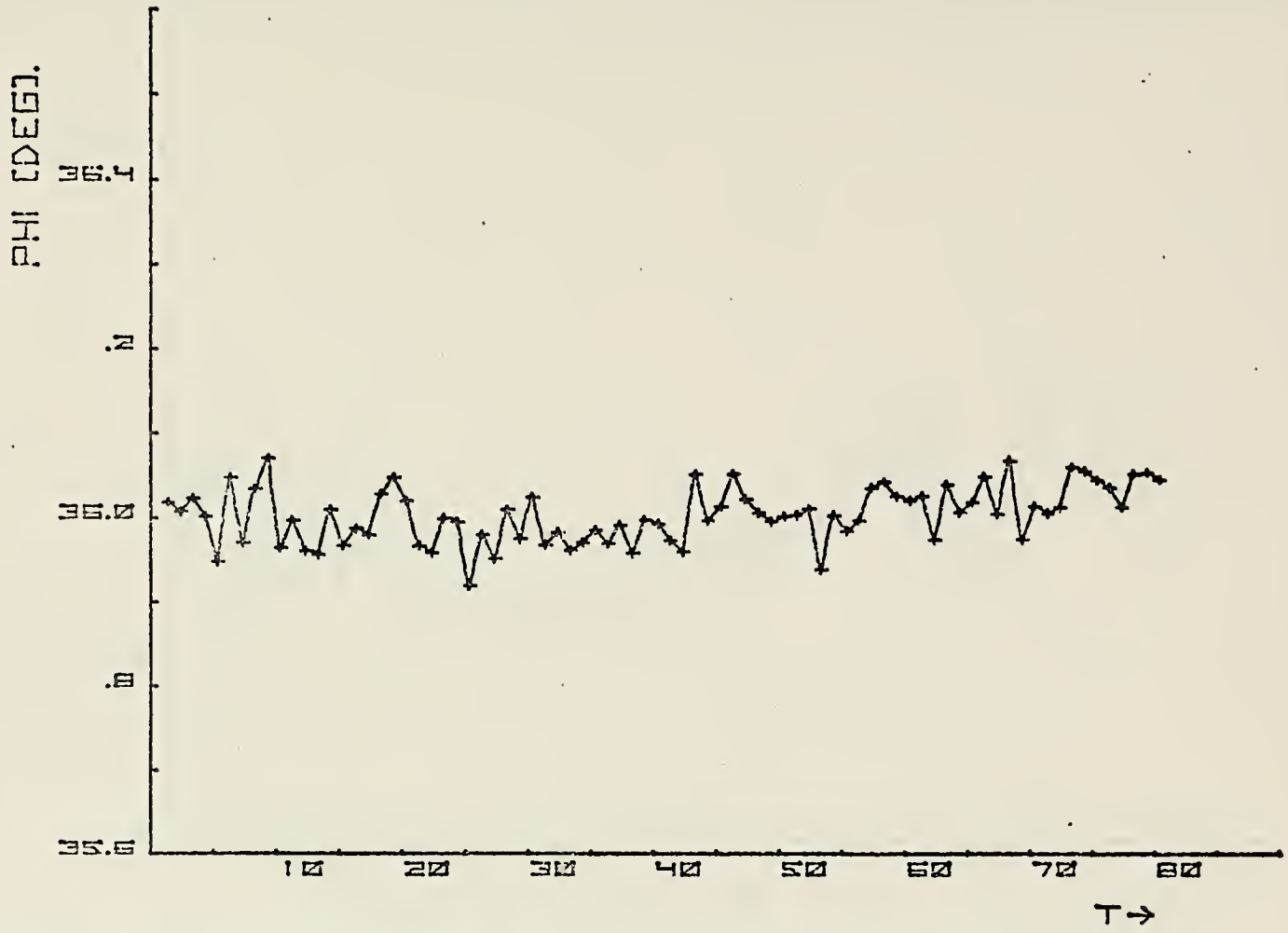

FIGURE 28. PHI, DRIFT CORRECTED, FROM COR COORDINATES, Station 1-25

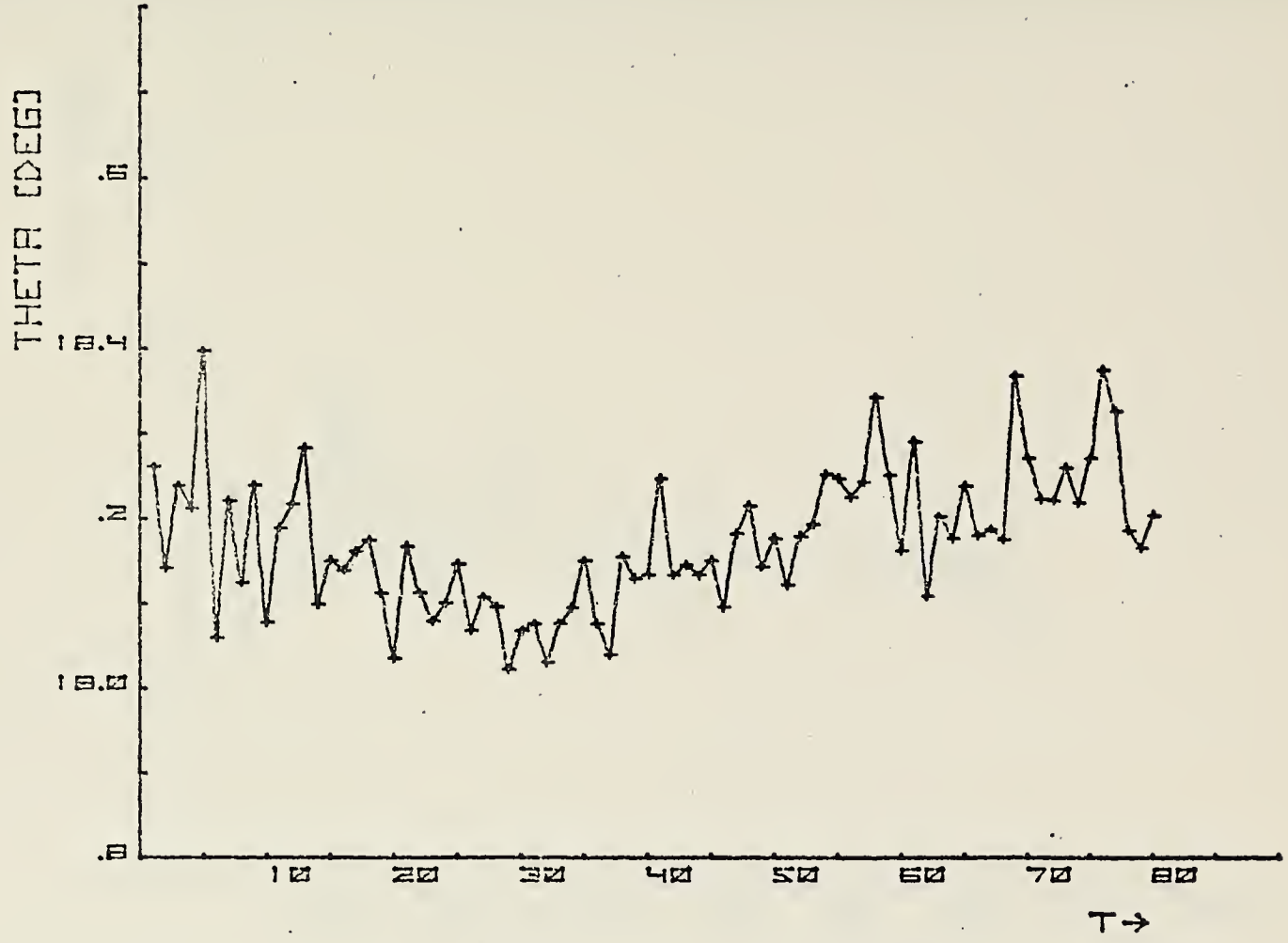

FIGURE 29. THETA, DRIFT CORRECTED, FROM COR COORDINATES, Station 1-25

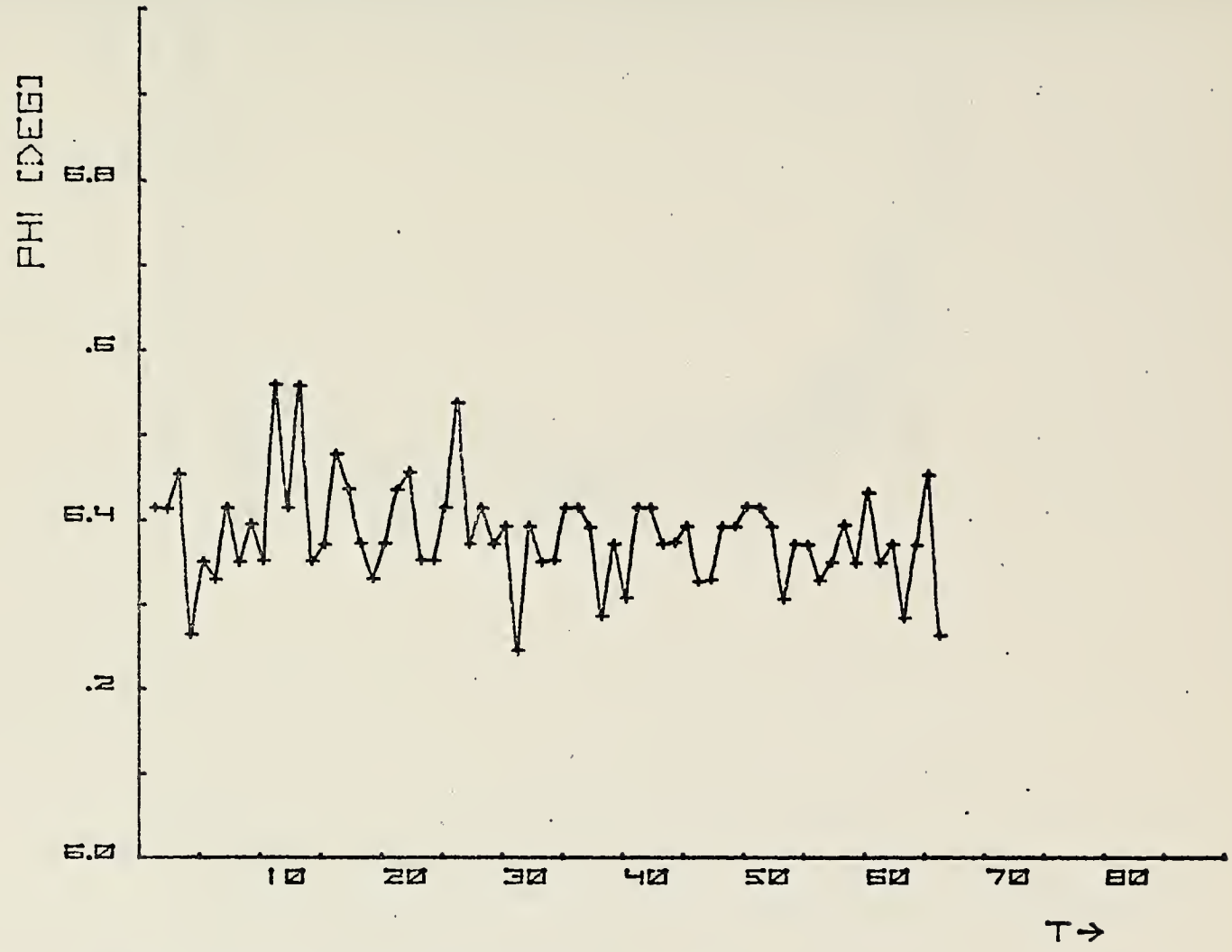

FIGURE 30, PHI, Station 6-50

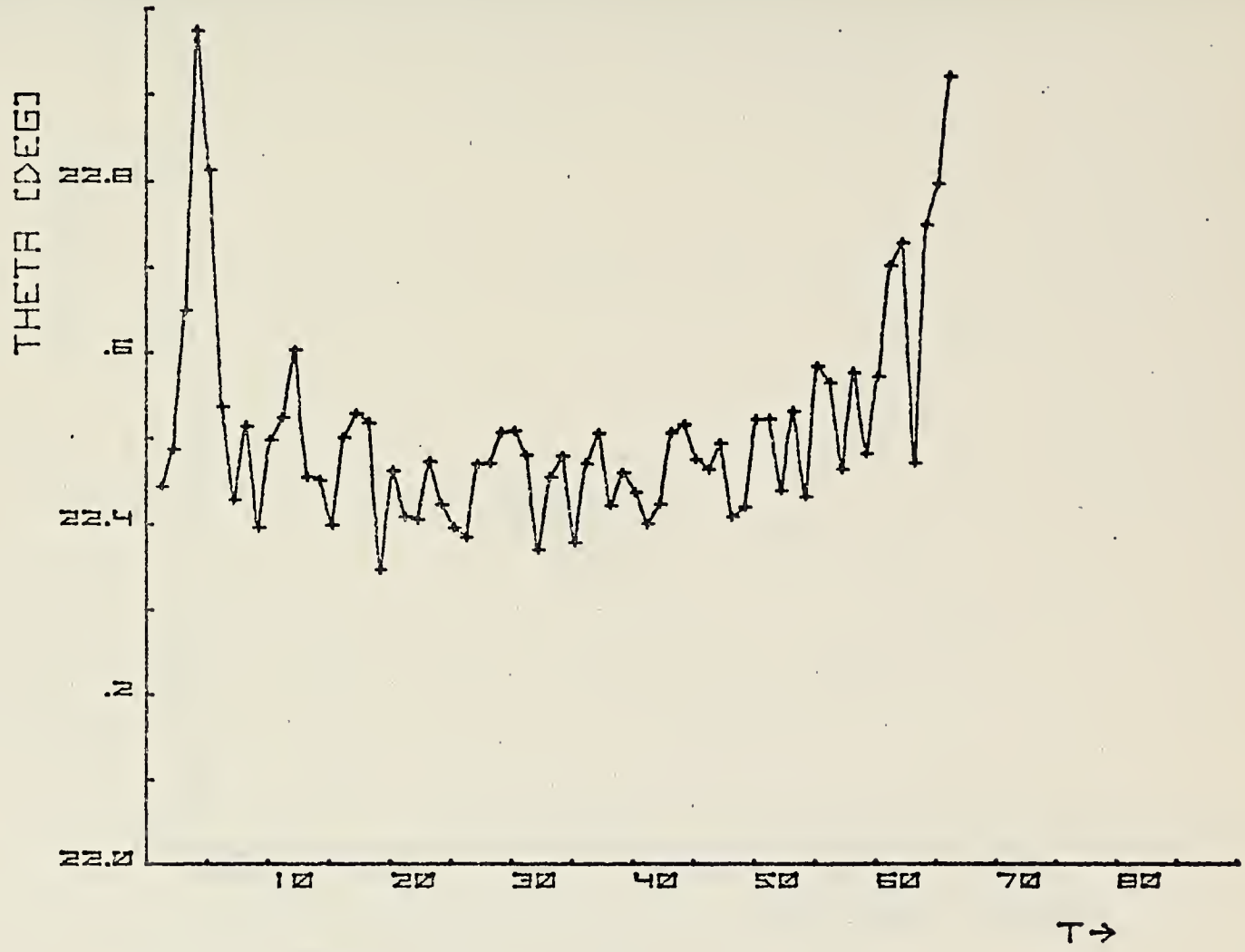

FIGURE 31, THETA, Station 6-50

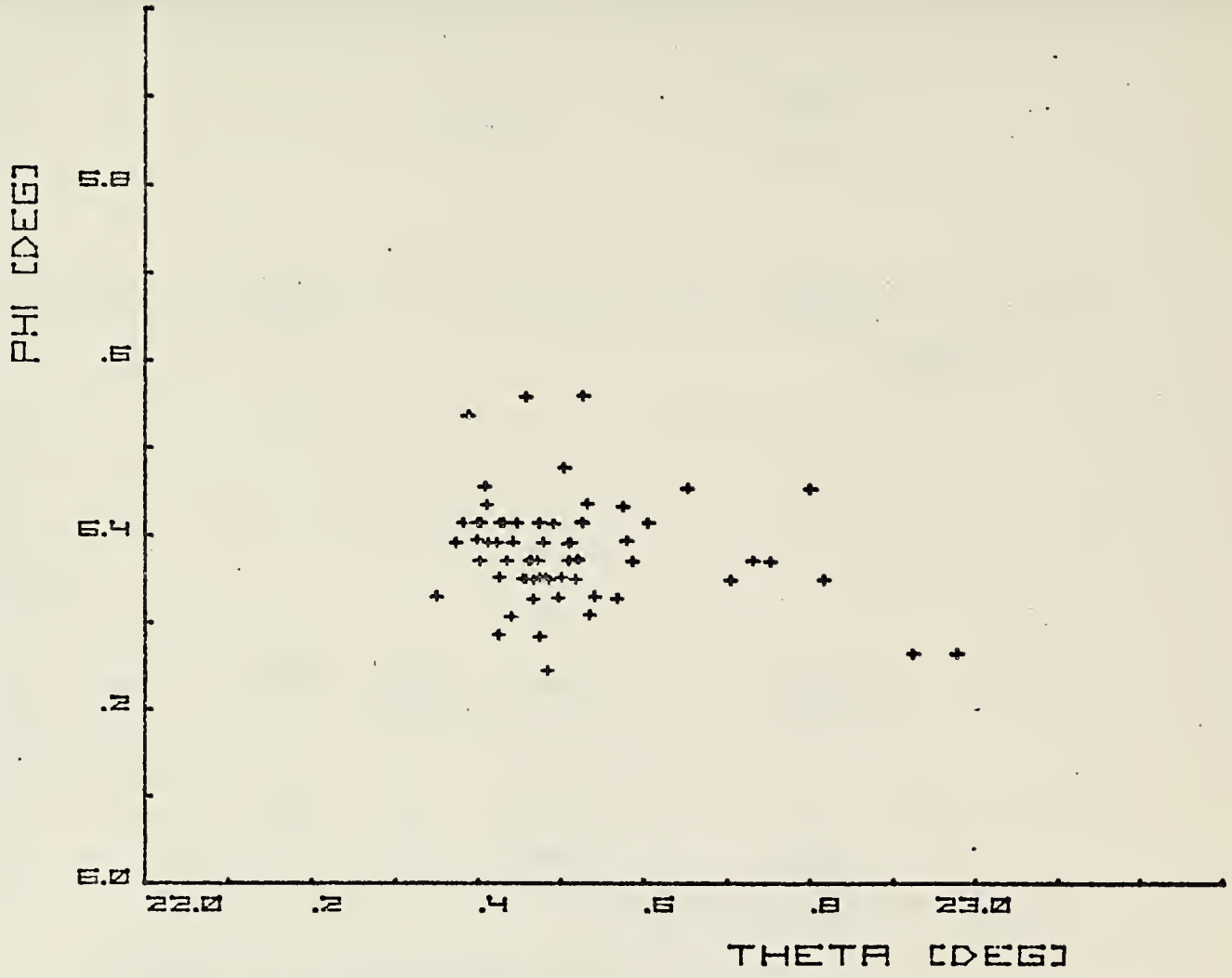

FIGURE 32. PHI vs. THETA, Station 6-50

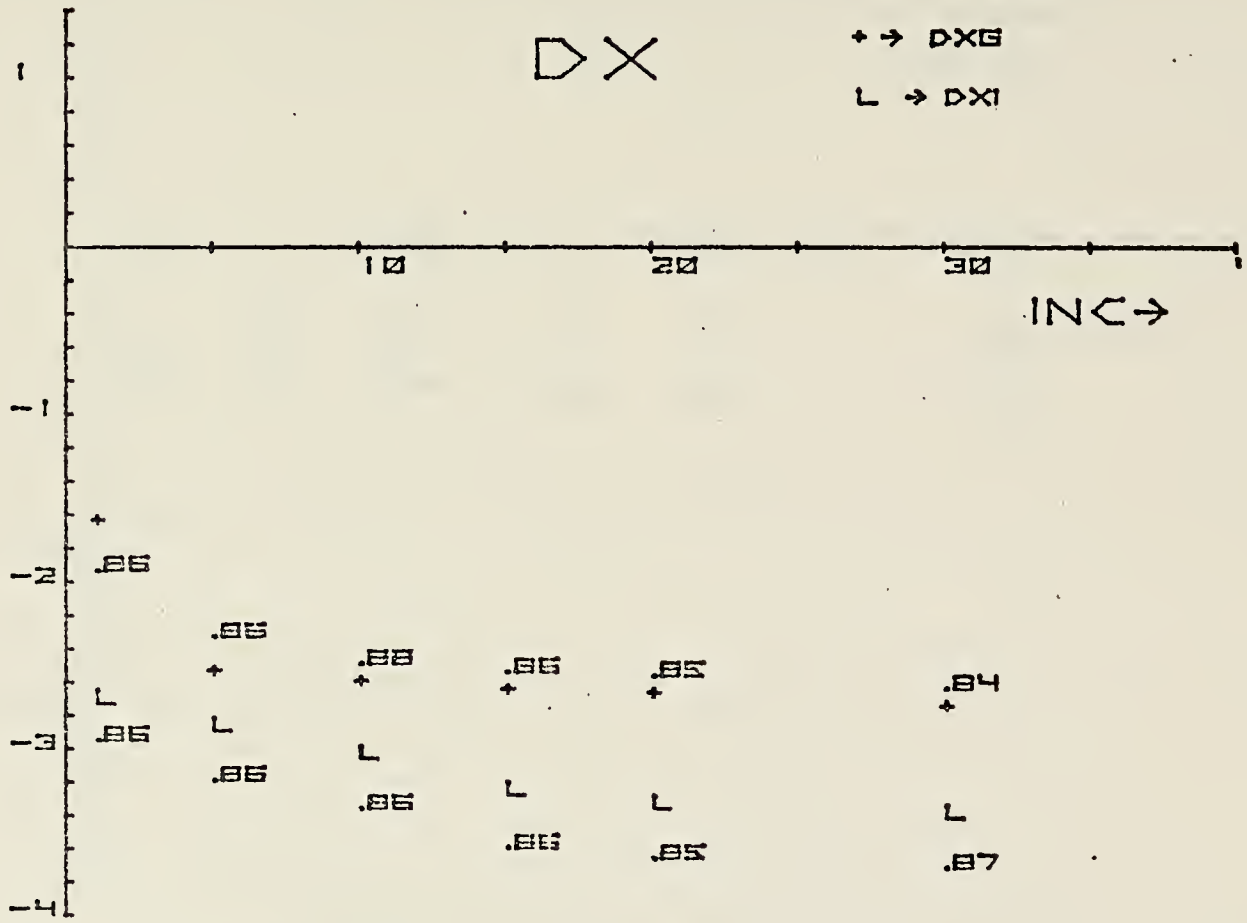

FIGURE 33. DX, Station 1-25

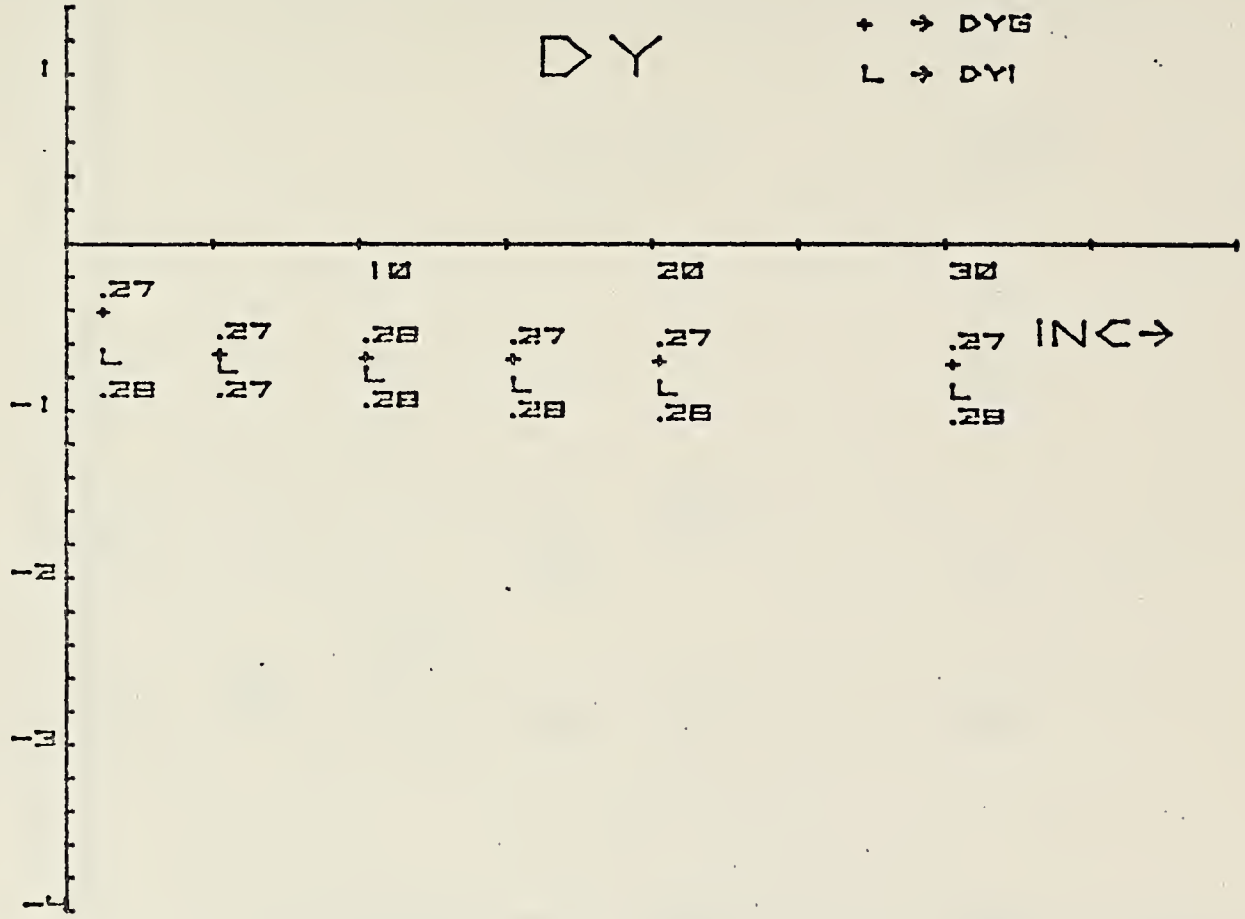

FIGURE 34. DY, Station 1-25

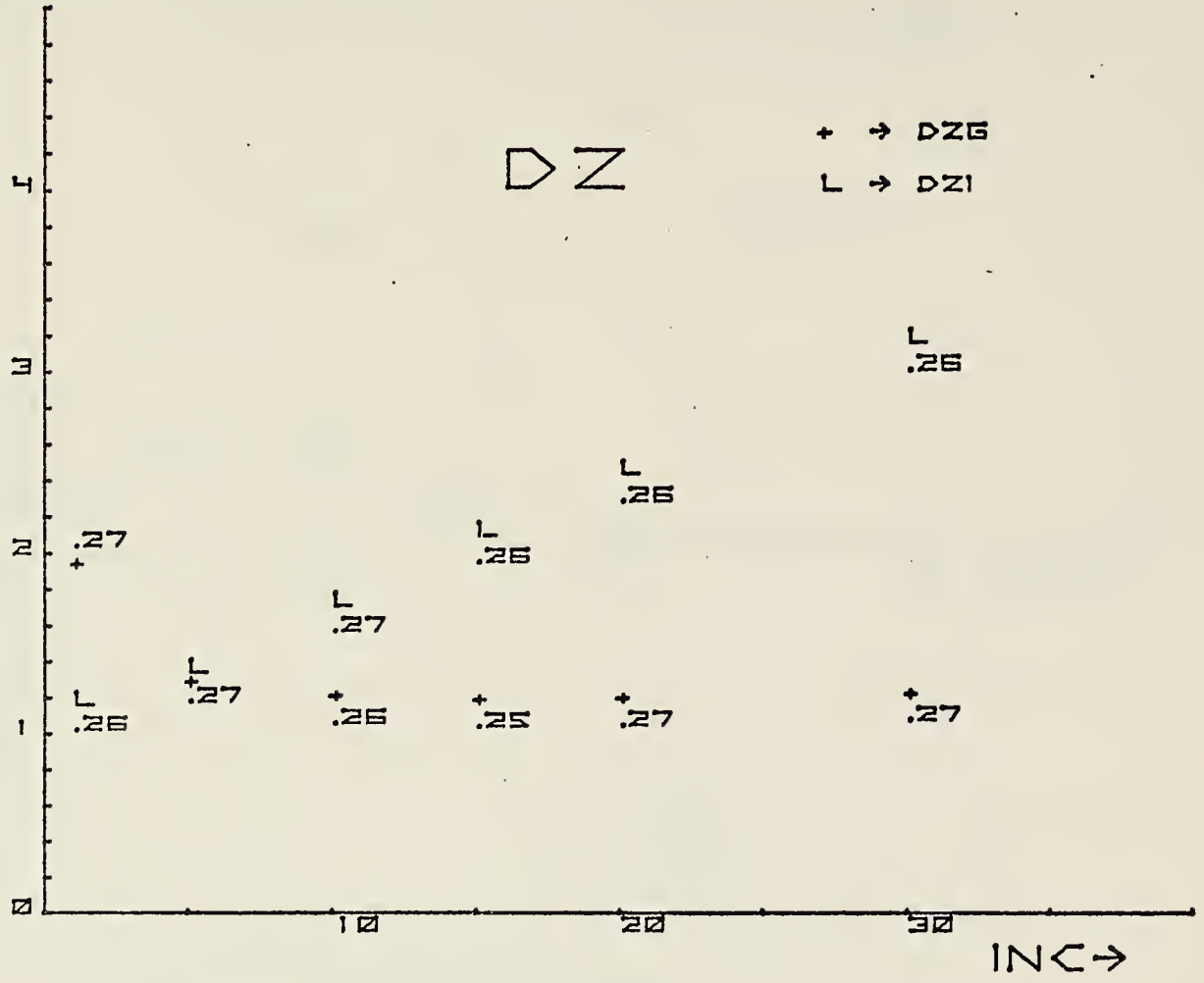

FIGURE 35. DZ, Station 1-25

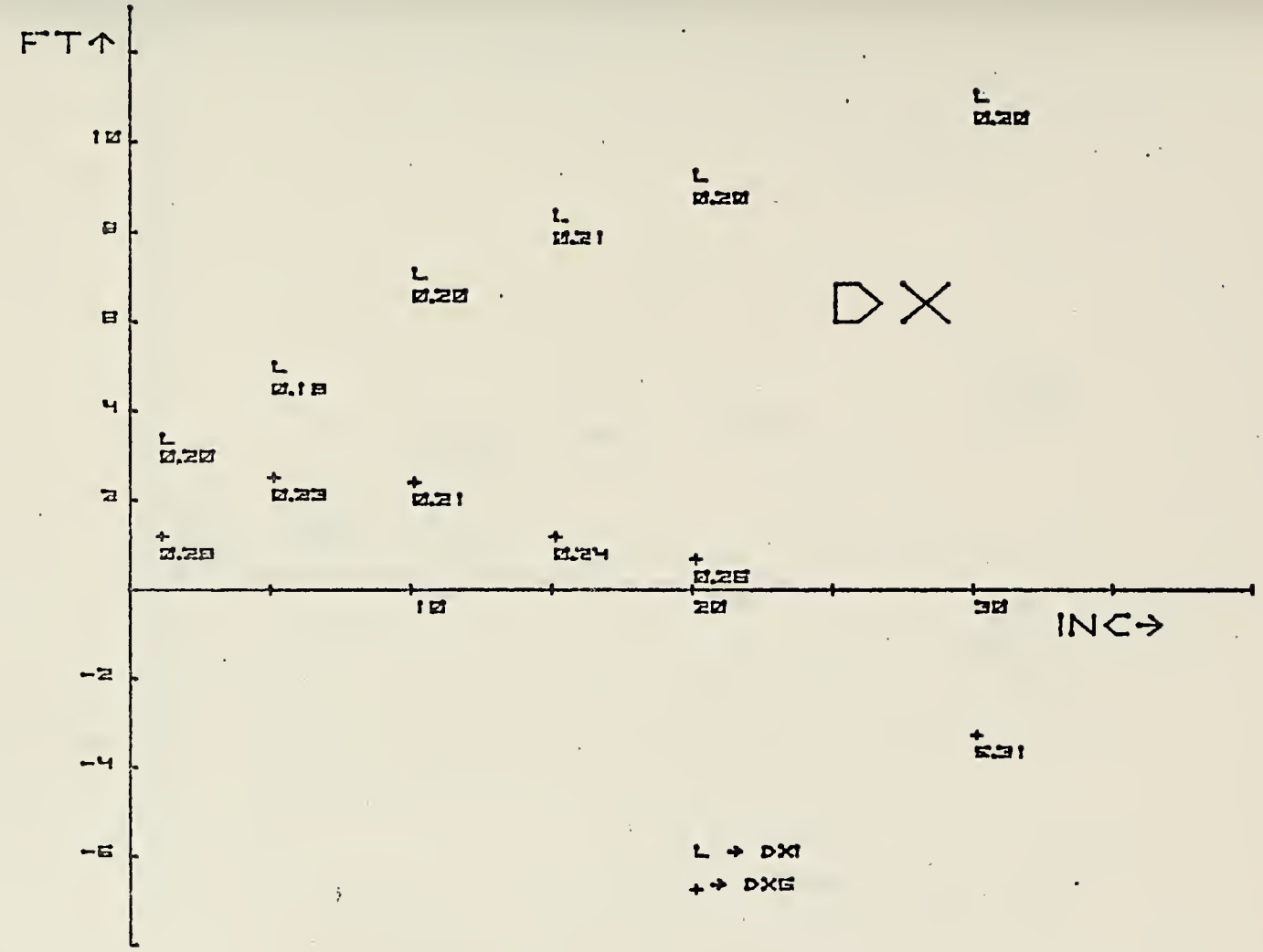

FIGURE 36. DX, Station 6-50

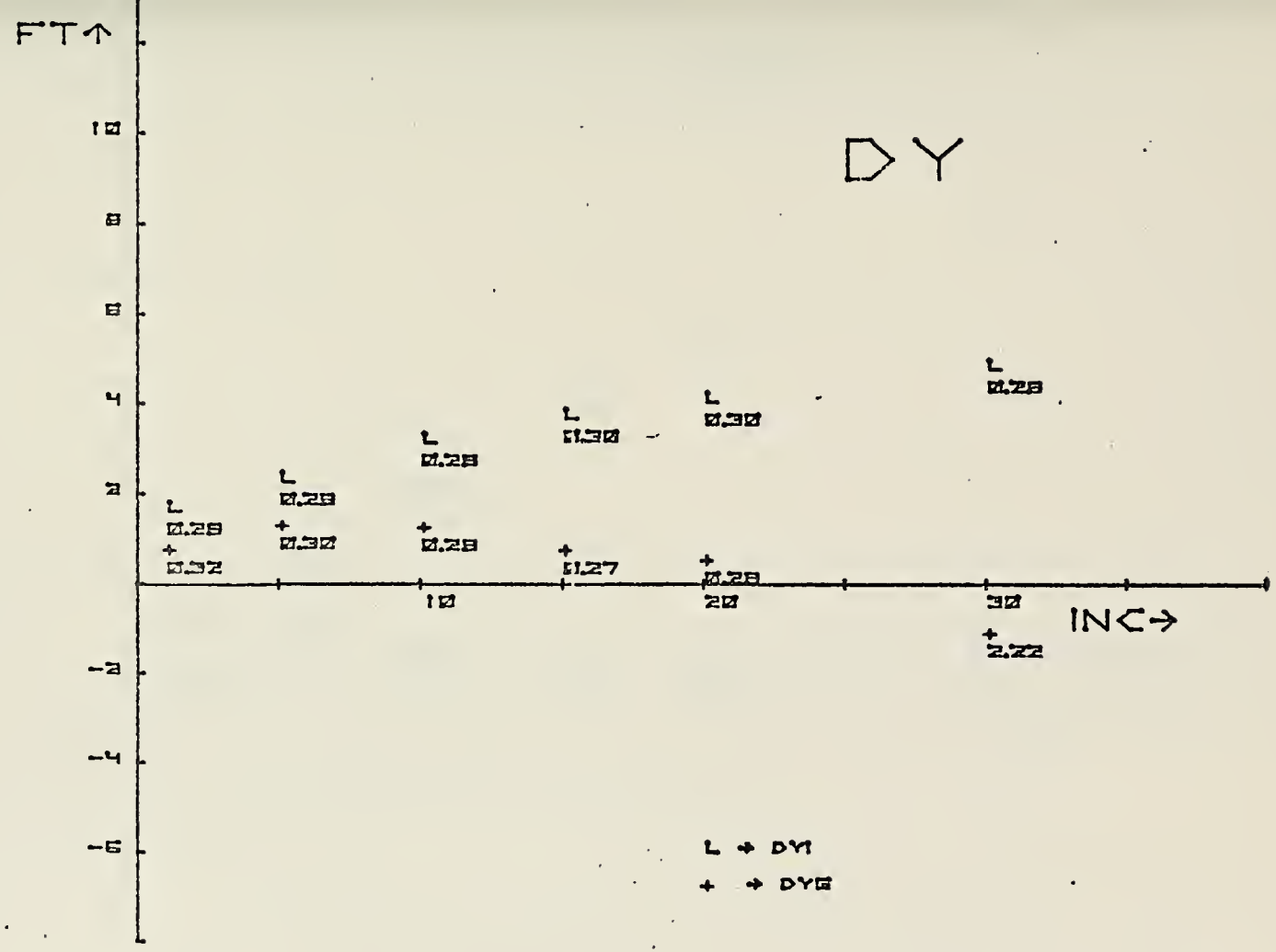

FIGURE 37. DY, Station 6-50

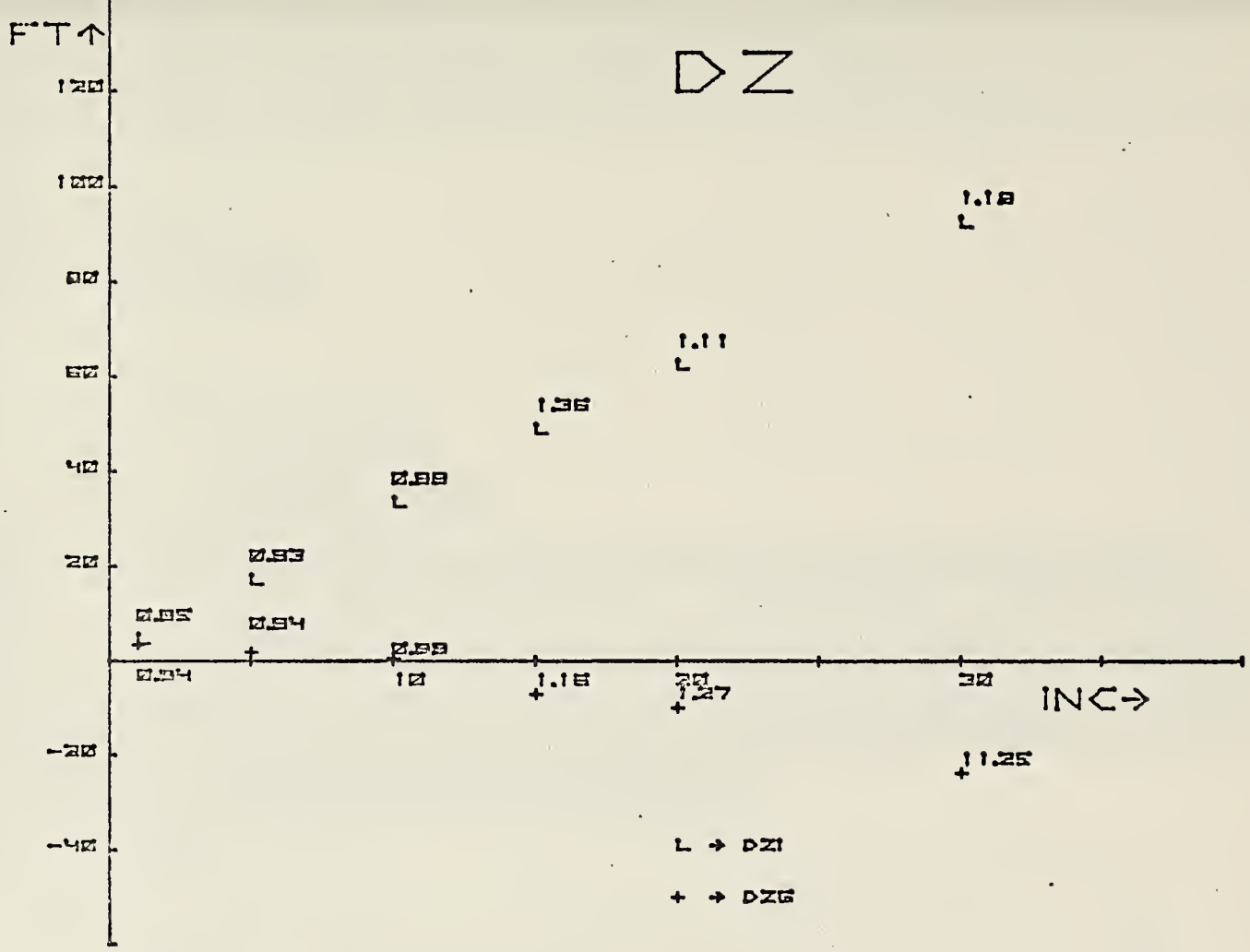

FIGURE 38. DZ, Station 6-50

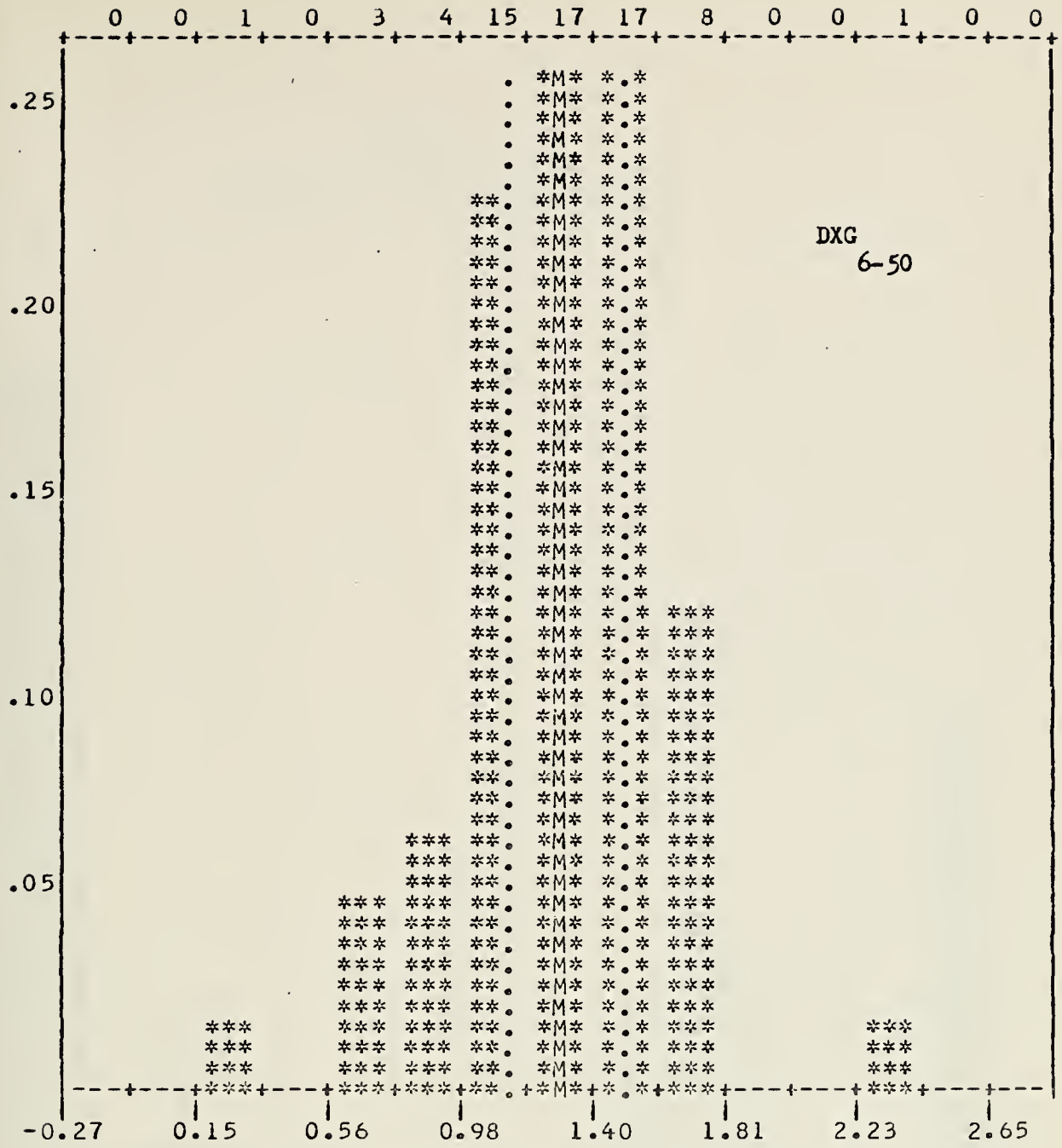

SCALE FIXED FROM -2.684946E-01 TO 2.855496E 00

CENTRAL TENDENCY		SPREAD	
MEAN	1.293501E 00	VARIANCE	9.909379E-02
MEDIAN	1.308594E 00	STD DEV	3.147917E-01
TRIMEAN	1.311523E 00	COEF VAR	2.433641E-01
MIDMEAN	1.308478E 00	MEAN DEV	2.421283E-01
MIDRANGE	1.253906E 00	RANGE	1.984375E 00
GEOM MEAN	1.246123E 00	MIDSPREAD	4.101563E-01
HARM MEAN	1.174641E 00		

FIGURE 39. DXG HISTOGRAM, Station 6-50

APPENDIX A

STUTRACK I COMPUTER PROGRAM

```
      DIMENSION DXI(150),DYI(150),DZI(150),DXG(150),DYG(150),DZG(150)
      DIMENSION V(150),SCX(2),SCY(2),SCZ(2),SCXG(2),SCYG(2),SCZG(2)
      DIMENSION DPH(150),U(150),A(150),X(150),Y(150),Z(150),XG(150)
      DIMENSION YG(150),ZG(150),RG(150),XI(150),YI(150),ZI(150),HI(150)
      TO=.000005
      INC=1
      AD=585.
      DO 100 I=1,100
      READ(5,101)DPH(I),V(I)
  101 FORMAT(2F10.0)
      WRITE(6,102)DPH(I),V(I)
  102 FORMAT(2F15.8)
      KK=I
      IF(DPH(I))103,103,100
  100 CONTINUE
  103 VO=4860.
      SDX=0.
      DT=0.
      SDY=0.
      SDZ=0.
      SDXG=0.
      SDYG=0.
      SDZG=0.
      DXSQ=0.
      DYSQ=0.
      DZSQ=0.
      DXGSQ=0.
      DYGSQ=0.
      DZGSQ=0.
      READ(5,38)TILTX,TILTY
      WRITE(6,38)TILTX,TILTY
   38 FORMAT(2F10.0)
      DO 1 I=1,150
      READ(5,2)IHMIN,ISEC,TX,TY,TZ,TC,RBNX,RBNY,RBNZ
    2 FORMAT(2I4,3F8.7,F7.6,3F6.1)
      IFLAG=0
      IF(IHMIN.EQ.9999)GO TO 99
      J=I
      RG(I)=0.
      ZG(I)=0.
      TI=0.
      ZI(I)=0.
      RI=0.
      TG=0.
      H1(I)=0.
      X(I)=((VO*VO)/60.)*(TC+TX-.0016)*(TC-TX)
      Y(I)=((VO*VO)/60.)*(TC+TY-.0016)*(TC-TY)
      Z(I)=((VO*VO)/60.)*(TC+TZ-.0016)*(TC-TZ)
```


APP A

```
      XO=X(I)
      YO=Y(I)
      XTILT=(TILTX-505.)*(.000145386)
      YTILT=(TILTY-505.)*(.000145386)
 8300 FORMAT(5F25.8)
      X(I)=X(I)-(Z(I)*SIN(XTILT))
      Y(I)=Y(I)-(Z(I)*SIN(YTILT))
      Z(I)=Z(I)+(XO*SIN(XTILT))+(YO*SIN(YTILT))
      S=(((X(I)*X(I))+(Y(I)*Y(I))+(Z(I)*Z(I)))**.5)
      AA=Z(I)/S
      A(1)=ARSIN(AA)
      H=S*COS(A(1))
      RC=((((X(I)+15.)**2)+((Y(I)+15.)**2)+((Z(I)+15.)**2))**.5)
      T=(TC*S)/RC
C   THE ISOGRADIENT COMPUTATIONS BEGIN HERE
      DO 5 K=1,KK,INC
      M=K+INC
      IF(M.GT.KK)GO TO 4700
      DZ=DPH(K)-DPH(M)
      G=(V(M)-V(K))/DZ
      DZO=DZ/2.
   12 AA=(((G*DZ)/V(K))+1.)*COS(A(K))
      A(M)=ARCOS(AA)
      T1=(COS(A(M))/(1.+SIN(A(M))))*((1.+SIN(A(K)))/COS(A(K)))
      DT=(1./G)*ALOG(T1)
      TG=TG+DT
      T2=T-TG
      T3=ABS(T2)
      IF(T3.LE.TO)GO TO 50
      IF(T2)51,50,50
   51 DZ=DZ-DZO
      TG=TG-DT
      DZO=DZO/2
      IFLAG=1
      GO TO 12
   50 DR=(-1.)*(V(K)/(G*COS(A(K))))*(SIN(A(M))-SIN(A(K)))
      RG(I)=RG(I)+DR
      ZG(I)=ZG(I)+DZ
      IF(T3.LE.TO)GO TO 52
      IF(IFLAG.NE.1)GO TO 5
   49 DZ=DZ-DZO
      DZO=DZO/2.
      GO TO 12
    5 CONTINUE
C THIS BEGINS THE ISOVELOCITY STEPS
   52 DO 6 K=1,KK,INC
      M=K+INC
      MM=M+INC
```

```
      IF(MM.GT.KK)GO TO 4700
      DZ=DPH(K)-DPH(M)
      DZO=DZ/2
   18 DS=DZ/SIN(A(K))
      VI=(V(K)+V(M))/2.
      VII=(V(M)+V(MM))/2.
      DT=DS/VI
      TI=TI+DT
      T2=T-TI
      T3=ABS(T2)
      IF(T3.LE.TO)GO TO 60
      IF(T2)61,60,60
   61 TI=TI-DT
      T4=DT-T3
      DS=T4*VI
      T3=0.0000
   60 DH=DS*COS(A(K))
      HI(I)=HI(I)+DH
      ZI(I)=ZI(I)+DZ
      AA=COS(A(K))*(VII/VI)
      A(M)=ARCOS(AA)
      IF(T3.LE.TO)GO TO 63
    6 CONTINUE
   63 XG(I)=(X(I)/H)*RG(I)
      YG(I)=(Y(I)/H)*RG(I)
      XI(I)=(X(I)/H)*HI(I)
      YI(I)=(Y(I)/H)*HI(I)
      DXI(I)=RBNX-XI(I)
      DYI(I)=RBNY-YI(I)
      DZI(I)=RBNZ-ZI(I)
      DXG(I)=RBNX-XG(I)
      DYG(I)=RBNY-YG(I)
      DZG(I)=RBNZ-ZG(I)
      SDX=SDX+DXI(I)
      SDY=SDY+DYI(I)
      SDZ=SDZ+DZI(I)
      SDXG=SDXG+DXG(I)
      SDYG=SDYG+DYG(I)
      SDZG=SDZG+DZG(I)
      DXSQ=DXSQ+(DXI(I)*DXI(I))
      DYSQ=DYSQ+(DYI(I)*DYI(I))
      DZSQ=DZSQ+(DZI(I)*DZI(I))
      DXGSQ=DXGSQ+(DXG(I)*DXG(I))
      DYGSQ=DYGSQ+(DYG(I)*DYG(I))
      DZGSQ=DZGSQ+(DZG(I)*DZG(I))
 8010 FORMAT(5X,6F20.8)
    1 CONTINUE
   99 AX=SDX/J
```

```
      AY=SDY/J
      AZ=SDZ/J
      AXG=SDXG/J
      AYG=SDYG/J
      AZG=SDZG/J
      VARX=(DXSQ/J)-(AX*AX)
      VARY=(DYSQ/J)-(AY*AY)
      VARZ=(DZSQ/J)-(AZ*AZ)
      VARXG=(DXGSQ/J)-(AXG*AXG)
      VARYG=(DYGSQ/J)-(AYG*AYG)
      VARZG=(DZGSQ/J)-(AZG*AZG)
      DEVX=SQRT(VARX)
      DEVY=SQRT(VARY)
      DEVZ=SQRT(VARZ)
      DEVXG=SQRT(VARXG)
      DEVYG=SQRT(VARYG)
      DEVZG=SQRT(VARZG)
      SCX(1)=AX-(5.*DEVX)
      SCX(2)=AX+(5.*DEVX)
      SCY(1)=AY-(5.*DEVY)
      SCY(2)=AY+(5.*DEVY)
      SCZ(1)=AZ-(5.*DEVZ)
      SCZ(2)=AZ+(5.*DEVZ)
      SCXG(1)=AXG-(5.*DEVXG)
      SCXG(2)=AXG+(5.*DEVXG)
      SCYG(1)=AYG-(5.*DEVYG)
      SCYG(2)=AYG+(5.*DEVYG)
      SCZG(1)=AZG-(5.*DEVZG)
      SCZG(2)=AZG+(5.*DEVZG)
    3 WRITE(6,20)
   20 FORMAT(15X,'DX',13X,'DY',13X,'DZ',13X,'DXG',12X,'DYG',12X,'DZG')
      DO 30 I=1,J
      WRITE(6,21)(DXI(I),DYI(I),DZI(I),DXG(I),DYG(I),DZG(I))
   21 FORMAT(5X,6F15.8)
   30 CONTINUE
      WRITE(6,34)
   34 FORMAT(5X,'XI',13X,'YI',13X,'ZI',13X,'XG',13X,'YG',13X,'ZG')
      DO 40 I=1,J
      WRITE(6,35)(XI(I),YI(I),ZI(I),XG(I),YG(I),ZG(I))
   35 FORMAT(6F15.8)
   40 CONTINUE
      NBAR=15
      N=J
      CALL FIX(SCX)
      CALL HISTF(DXI,N,NBAR)
      CALL FIX(SCY)
      CALL HISTF(DYI,N,NBAR)
      CALL FIX(SCZ)
```

```
      CALL HISTF(DZI,N,NBAR)
      CALL FIX(SCXG)
      CALL HISTF(DXG,N,NBAR)
      CALL FIX(SCYG)
      CALL HISTF(DYG,N,NBAR)
      CALL FIX(SCZG)
      CALL HISTF(DZG,N,NBAR)
      GO TO 4800
4700  WRITE(6,4701)
4701  FORMAT(5X,'YOU HAVE MADE AN ERROR IN CHOOSING INC')
4800  STOP
      END
```

BIBLIOGRAPHY

1. Kinsler, L. E. and Frey, A. R., Fundamentals of Acoustics, 2d ed., John Wiley & Sons, Inc., 1962.

2. Medwin, H., "Sound Fluctuations In The Upper Ocean," J. Acoust. Soc. Am., v. 56, p. 1105-1110, 6 October, 1974.

3. Research and Engineering Department, Instrumentation Division, Range Systems Branch, Mathematics of Acoustic 3-D Tracking (NUTRACK III), by J. W. E. Edmonson and D. L. Pearson, p. 15, 24 November 1969.

4. Naval Torpedo Station Report 1030, NAVTORPSTA Range Users Manual, by A. E. Anunson, p. 125, 20 April, 1971.

5. Naval Ordnance Systems Command, Description and Operation, 3-D Range Equipment, by J. E. Udd, p. 36, 15 February 1973.

6. Naval Torpedo Station Report 845, Digital Velocimeter System Operation Manual, by R. A. Daniel and D. L. Pearson, p. 77, November 1967.

7. Naval Torpedo Station Report 1154, Autotape Accuracy and Water Reflection Problems, by G. A. Anunson, p. 47, January, 1972.

INITIAL DISTRIBUTION LIST

		No. Copies
1.	Defense Documentation Center Cameron Station Alexandria, Virginia 22314	2
2.	Library, Code 0212 Naval Postgraduate School Monterey, California 93940	2
3.	Department Chairman, Code 61 Department of Physics Naval Postgraduate School Monterey, California 93940	2
4.	Professor James V. Sanders Department of Physics Naval Postgraduate School Monterey, California 93940	1
5.	Professor C.E. Menneken Department of Electrical Engineering Naval Postgraduate School Monterey, California 93940	3
6.	Lt. Stuart C. Karon USN U.S. Naval Destroyer School Newport, R.I. 02840	1
7.	Lt. Victor J. Bankston USN SMC 2521 Naval Postgraduate School Monterey, California 93940	1

Thesis 156432
K1445 Karon
c.1 Ray trace experiment
on the underwater range
at Dabob Bay.